Area per Lipid and Acyl Length Distributions in Fluid Phosphatidylcholines Determined by ^{2}H NMR Spectroscopy

Horia I. Petrache,* Steven W. Dodd,† and Michael F. Brown†

*Department of Physiology, Johns Hopkins University School of Medicine, Baltimore, Maryland 21205, and †Department of Chemistry, University of Arizona, Tucson, Arizona 85721

ABSTRACT Deuterium (^{2}H) NMR spectroscopy provides detailed information regarding the structural fluctuations of lipid bilayers, including both the equilibrium properties and dynamics. Experimental ^{2}H NMR measurements for the homologous series of 1,2-diacyl-*sn*-glycero-3-phosphocholines with perdeuterated saturated chains (from C12:0 to C18:0) have been performed on randomly oriented, fully hydrated multilamellar samples. For each lipid, the C–D bond order parameters have been calculated from de-Paked ^{2}H NMR spectra as a function of temperature. The experimental order parameters were analyzed using a mean-torque potential model for the acyl chain segment distributions, and comparison was made with the conventional diamond lattice approach. Statistical mechanical principles were used to relate the measured order parameters to the lipid bilayer structural parameters: the hydrocarbon thickness and the mean interfacial area per lipid. At fixed temperature, the area decreases with increasing acyl length, indicating increased van der Waals attraction for longer lipid chains. However, the main effect of increasing the acyl chain length is on the hydrocarbon thickness rather than on the area per lipid. Expansion coefficients of the structural parameters are reported and interpreted using an empirical free energy function that describes the force balance in fluid bilayers. At the same absolute temperature, the phosphatidylcholine (PC) series exhibits a universal chain packing profile that differs from that of phosphatidylethanolamines (PE). Hence, the lateral packing of phospholipids is more sensitive to the headgroup methylation than to the acyl chain length. A fit to the area per lipid for the PC series using the empirical free energy function shows that the PE area represents a limiting value for the packing of fluid acyl chains.

INTRODUCTION

A comprehensive understanding of structure–function relations of biomembranes ultimately relies on knowledge of the properties of lipid bilayers in relation to lipid–protein interactions. The complex structural dynamics of membranes involve a balance of forces characteristic of amphiphilic systems, as manifested by both the protein and lipid structural parameters and their connection to specific biomembrane functions (Brown, 1994; Epand, 1998; Bezrukov et al., 1998; White and Wimley, 1999). One quantity that describes the bilayer microstructure with regard to molecular packing is the average interfacial area per lipid molecule $\langle A \rangle$, which is defined in reference to the average hydrocarbon thickness D_C and the hydrocarbon chain volume V_C. The precise values of these lipid structural parameters are determined by the interactions between the various lipid bilayer constituents, and their measurement provides a practical way to acquire information on the intermolecular interactions. By studying the interaction of lipid molecules, one is better positioned to further explore more complex systems, such as lipid–protein assemblies, in terms of the effect of membrane components on the bilayer thermodynamic parameters, and, in particular, on the area per lipid.

The question is thus how to obtain accurate estimates of structural parameters for the disordered, but biologically relevant fluid state as a mean of relating the bilayer microstructure to the characteristic force balance responsible for lipid self-assembly. In this regard, the most powerful biophysical techniques are small-angle X-ray scattering (Tardieu et al., 1973; Worthington et al., 1973; Lewis and Engelman, 1983; McIntosh and Simon, 1986; Rand and Parsegian, 1989), small-angle neutron scattering (Zaccai et al., 1979; Wiener and White, 1992; Lemmich et al., 1996), Fourier transform infrared spectroscopy (FTIR) (Mendelsohn et al., 1989; Davies et al., 1992; Tuchtenhagen et al., 1994), and deuterium (^{2}H) NMR spectroscopy (Seelig and Seelig, 1974; De Young and Dill, 1988; Ipsen et al., 1990; Thurmond et al., 1991; Koenig et al., 1997). Moreover, computer simulations of lipid bilayers are useful in revealing important details of the structural dynamics in terms of the underlying force fields (Pastor and Feller, 1996). The structural parameters D_C and $\langle A \rangle$ can be directly determined from scattering experiments in special cases where relatively high positional ordering of membrane components is present (Nagle and Wiener, 1988; Tristram-Nagle et al., 1993; Sun et al., 1994). More often though, especially in the fluid state at full hydration, the direct measurement of the area per lipid using scattering techniques is a much more difficult task, even for pure lipid bilayers (McIntosh and Simon, 1986; Nagle et al., 1996; Koenig et al., 1997; Petrache et al., 1998a; Tristram-Nagle et al., 1998).

Deuterium NMR spectroscopy has been a powerful tool for investigations of biological membranes. Although it

Received for publication 5 June 2000 and in final form 12 September 2000.

Address reprint requests to Michael F. Brown, Department of Chemistry, University of Arizona, Tucson, AZ 85721. Tel.: 520-621-2163; Fax: 520-621-8407; E-mail: mfbrown@u.arizona.edu.

0006-3495/00/12/3172/21 $2.00

measures orientational ordering as opposed to positional order, it reveals detailed aspects with regard to the lipid chain packing from which structural parameters can be obtained. Since its early use (Seelig and Seelig, 1974; Mely et al., 1975), ^{2}H NMR has provided a wealth of information regarding the organization of membrane components, especially in regard to the lipid polar headgroups (Brown and Seelig, 1977, 1978) and acyl chains (Seelig, 1977; Salmon et al., 1987). The ^{2}H NMR order profile of the acyl chains is very sensitive to physicochemical conditions, such as temperature, concentration, and hydration level, and therefore it has been used to measure the response of the membrane to these various factors (Bloom et al., 1991; Jansson et al., 1992; Morrow et al., 1992; Koenig et al., 1997). Another important use of ^{2}H NMR spectra of lipid acyl chains is to describe the influences of membrane components, such as cholesterol (Oldfield et al., 1978; Trouard et al., 1999) and hydrophobic peptides (De Planque et al., 1998; Koenig et al., 1999), on the lipid bilayer. For a complete understanding of these effects one needs to relate the measured ^{2}H NMR spectra to physical properties of the lipid chains.

A quantitative interpretation of the order parameters in terms of membrane thermodynamic parameters and, in particular, the membrane structure has been particularly challenging. This is because the complexity of the lipid bilayer (i.e., the large number of degrees of freedom) makes statistical mechanical calculations starting from first principles intractable (see Nagle, 1980, for a review). As a result, simplified chain conformation models have been considered, which attempt to capture the most relevant degrees of freedom in terms of the appropriate distributions. One example is the diamond lattice model (Seelig and Seelig, 1974; Salmon et al., 1987), from which one obtains a simple linear relationship between the ^{2}H NMR order parameter $S_{CD}^{(i)}$ of the chain segment (i), and the corresponding projection $\langle D_i \rangle$ along the membrane normal (Schindler and Seelig, 1975; Salmon et al., 1987; Thurmond et al., 1991; Nagle, 1993; Douliez et al., 1995), namely,

$$\frac{\langle D_i \rangle}{D_M} = \frac{1}{2} - S_{CD}^{(i)}. \qquad (1)$$

Here, D_i is the distance between carbons $i + 1$ and $i - 1$, projected on the bilayer normal, and $D_M = 2.54$ Å is the maximum possible projection. The brackets in Eq. 1 represent an ensemble average over chain conformations. By summing over consecutive chain segments (i), one can calculate the full chain projection, or partial distances between different carbon atoms along the chain. Knowing the chain length, the area per lipid can then be calculated by using information on the chain volume (Thurmond et al., 1991; Nagle, 1993; Brown, 1996). Convenient as it is, Eq. 1 is nonetheless an unexpected result, because the order parameter is a quadratic function of the segment tilt (the second-order Legendre polynomial). Clearly, Eq. 1 is a linear approximation of the real underlying relationship between $\langle D_i \rangle$ and $S_{CD}^{(i)}$. This linear form has proved to be quite effective in the past, giving results in fairly good agreement with scattering experiments that measure structural parameters more directly. But with newer and more precise measurements, discrepancies between the analysis of ^{2}H NMR and X-ray data regarding the area per lipid have become increasingly noticeable (Koenig et al., 1997; Petrache et al., 1999). Consequently, Eq. 1 and other similar linear relationships are open to reevaluation.

An alternative to the diamond lattice model was recently proposed by Petrache et al. (1999). Rather than considering a discrete set of segmental conformations, corresponding to the most populated internal dihedral angles, the new model is based on a continuum distribution of segmental orientations. This continuum distribution, here denoted by $f(D)$, is generated by the combined effect of internal degrees of freedom (dihedral angles) and chain motion as a whole (chain tilt). Based on this model, a new analytical relation was derived (Petrache et al., 1999), namely

$$\frac{\langle D_i \rangle}{D_M} = \frac{1}{2}\left(1 + \sqrt{\frac{-8S_{CD}^{(i)} - 1}{3}}\right), \qquad (2)$$

where the brackets indicate the ensemble average generated by the orientational distribution function $f(D)$. This expression has been shown to work better than the diamond lattice result for the calculation of chain segment projections (Petrache et al., 1999; Smondyrev and Berkowitz, 1999). However, when further applied to estimate the area per lipid using ^{2}H NMR data, it gave discrepancies with accepted X-ray results (Petrache et al., 1999).

The calculation of the area per lipid $\langle A \rangle$ from ^{2}H NMR data is unfortunately not straightforward, starting with the definition of the area itself. Although various moments of the distribution $f(D)$, in particular the average projection $\langle D \rangle$, can be defined and calculated in a straightforward manner, the same is not true for the average area $\langle A \rangle$. One possible approach to connecting the geometrical properties along the bilayer normal D and perpendicular to the bilayer normal $\langle A \rangle$ is to define an instantaneous area $A \equiv 4V_{CH_2}/D$, where V_{CH_2} denotes the volume of the chain segment. Then, as pointed out by Jansson et al. (1992), the calculation of the average area $\langle A \rangle$ amounts to calculation of $\langle 1/D \rangle$. The evaluation of $\langle 1/D \rangle$ requires knowledge of the functional form of the distribution function $f(D)$, or alternatively, knowledge of the moments of $f(D)$, as discussed by Jansson et al. (1992) and Petrache et al. (1999). Here we propose a methodology for area calculation that takes advantage of the continuum description of segmental conformations. It is important to note that continuum models have been extensively used in the analysis of NMR relaxation data (Brown, 1982; Halle, 1991; Trouard et al., 1994; Brown and Chan, 1995; Althoff et al., 1996; Nevzorov et al., 1998), whereas the analysis of

order parameters has tended to involve discrete descriptions. It is therefore desirable to combine the relaxation and order parameter analyses into a more consistent picture.

In what follows, we present the results of an extensive series of experimental ^{2}H NMR measurements of disaturated phospholipids in the fluid lamellar (L_α) state. Motivated by this ^{2}H NMR data set, and by recent X-ray scattering measurements (Nagle et al., 1996; Koenig et al., 1997; Petrache et al., 1998a), we then reformulate the continuum theory in terms of an effective orientational potential (mean-torque potential) (Brown, 1996). The latter is related to the distribution function for the segment orientations, and provides insight into the intermolecular interactions that govern the microstructure of phospholipid/water dispersions. Finally, the experimental data are interpreted in terms of the theory to yield a new conceptual framework for the analysis of bilayer structural properties.

EXPERIMENTAL METHODS

Phospholipid synthesis and sample preparation

High purity (≥99%) fatty acids were obtained from Sigma (St. Louis, MO) and were perdeuterated by catalytic exchange of ^{2}H for ^{1}H over a 10% Pd-charcoal catalyst (Aldrich, Milwaukee, WI) at 200°C. The perdeuterated fatty acids were more than 99% pure by gas–liquid chromatography on 10% SP-2330 (Supelco, Bellafonte, PA), and were typically 92–96% labeled with ^{2}H according to mass spectrometry. Symmetric (like chain) phospholipids were synthesized from the cadmium chloride adduct of *sn*-glycero-3-phosphocholine and the corresponding perdeuterated fatty acid anhydrides, as described by Salmon et al. (1987). Representative yields based on *sn*-glycero-3-phosphocholine were 75–90%. The asymmetric phosphatidylcholine, 1-palmitoyl-2-perdeuteriopalmitoyl-*sn*-glycero-3-phosphocholine (DPPC-d_{31}), in which the *sn*-2 chain was perdeuterated, was synthesized as follows. First, DPPC was reacted with snake venom phospholipase A_2 (Sigma); the resulting 1-palmitoyl-*sn*-glycero-3-phosphocholine was purified by column chromatography, and finally the lyso phosphatidylcholine was reacylated at the *sn*-2 position using the anhydride of perdeuteriopalmitic acid. After purification by column chromatography on silicic acid, all phospholipids gave single spots upon thin-layer chromatography in $CHCl_3$:MeOH:H_2O (65/35/5) followed by charring with 40% H_2SO_4 in EtOH.

Multilamellar samples were prepared by vortexing ~100–150 mg phospholipid together with an equal weight of ^{2}H-depleted ^1H_2O (Aldrich) above the bilayer phase transition temperature. The 50 wt % multilamellar dispersions were then centrifuged and sealed in cutoff ~6 or 10-mm-diameter Kimax- or Pyrex-type glass culture tubes with Teflon plugs. The samples were stored at −85°C when not in use.

Deuterium NMR methods

Deuterium NMR spectroscopy of the multilamellar lipid dispersions involved generation of the solid (quadrupolar) echo followed by Fourier transformation. Measurements were performed at 55.43 MHz with a phase-cycled, quadrupolar echo sequence, $(\pi/2)_x - \tau_2 - (\pi/2)_y - \tau_2 -$ acquire. A homebuilt ^{2}H NMR probe was used having a horizontal solenoidal radiofrequency coil design together with high-voltage capacitors (Polyflon, Norwalk, CT). A kilowatt radiofrequency boost amplifier (Model Tempo 2006, Henry Radio, Los Angeles, CA) was used in series with the spectrometer output to enable 90° pulse durations <3–4 μs for the 10-mm radiofrequency coil. The transient NMR signals were shunted to the preamplifier (Miteq, Hauppauge, NY) using a Lowe-Tarr series crossed diode circuit, and were acquired with a fast digitizer. Typical spectral acquisition parameters involved a pulse spacing (τ_2) of 40 μs, a dwell time of 2 μs (spectral width of ±250 kHz), and collection of 2048 data points. Recycle times were generally 1 s, and typically 600–2400 transients were collected, apodized by exponential multiplication (100-Hz line-broadening), and Fourier transformed beginning at the maximum of the solid echo. Both quadrature channels were used and the spectra were not symmetrized. The sample temperature was monitored before and after each measurement with a thermistor inserted directly above the radiofrequency coil, and was usually found to vary by less than 0.5°C during a given run. The temperatures are estimated accurate to within ±1°C of the reported values. All samples were subsequently checked by thin-layer chromatography and revealed no contamination or degradation.

Data analysis and reduction: Spectral assignments

The ^{2}H NMR spectral powder patterns were numerically deconvoluted (de-Paked) to yield the $\theta = 0°$ oriented spectra as described (Bloom et al., 1981). The most useful characteristic of the de-Pakeing algorithm is that it leads to increased spectral resolution. In addition, it reveals the "Me-2-3-2" spectral pattern (see below) and the large "plateau" peak, which are characteristic of perdeuterated disaturated phosphatidylcholines (see Fig. 1). Spectral assignments for multilamellar dispersions of 1,2-diperdeuteriomyristoyl-*sn*-glycero-3-phosphocholine (DMPC-d_{54}) and 1,2-diperdeuteriopalmitoyl-*sn*-glycero-3-phosphocholine (DPPC-d_{62}) were made by comparison to ^{2}H NMR results for the corresponding specifically deuterated phospholipids (Seelig and Seelig, 1974; Oldfield et al., 1978). For DPPC-d_{62}, assignments of the splittings due to the *sn*-1 and *sn*-2 chains entailed comparison of the de-Paked ^{2}H NMR spectra of DPPC-d_{62} (both

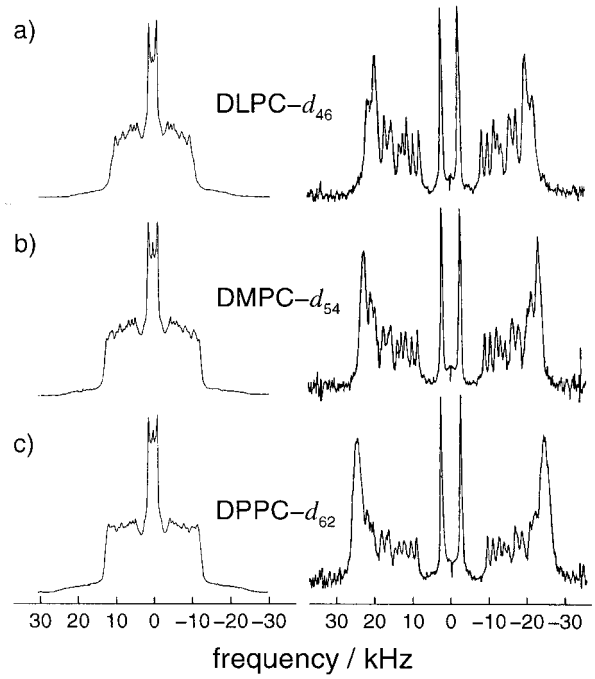

FIGURE 1 (*a–c*) Representative ^{2}H NMR spectra of homologous series of disaturated phosphatidylcholines with perdeuterated acyl chains. Samples were fully hydrated and were in the lamellar fluid phase at 50°C. Powder-type ^{2}H NMR spectra are shown at left, and the corresponding de-Paked ^{2}H NMR spectra at right.

chains deuterated) to DPPC-d_{31} (*sn*-2 chain deuterated). It was assumed that similar splittings occur for the other phosphatidylcholines, viz. 1,2-diperdeuteriolauroyl-*sn*-glycero-3-phosphocholine (DLPC-d_{46}), DMPC-d_{54}, and 1,2-diperdeuteriostearoyl-*sn*-glycero-3-phosphocholine (DSPC-d_{70}). Further peak assignments were made assuming the order parameters decrease in magnitude from C_2 (α carbon) to the methyl end, and that the area under each peak is proportional to the number of deuterons generating the peak (Williams et al., 1985). The only exception was the C_2 segment of the *sn*-2 chain, for which the splittings were assigned in the case of DPPC-d_{62} based on literature data for specifically deuterated lipids (Seelig and Seelig, 1974); it was assumed that the other lipids yielded similar C_2 splittings. Additionally, the assignments were made from the methyl terminus toward the plateau region. The terminal methyl groups possess the smallest quadrupolar splittings, and hence are the simplest to assign. The "2-3-2" pattern is then readily assigned, followed by the remainder of the fatty acyl chains.

The C–D bond order parameters, $S_{CD}^{(i)}$, of the de-Paked ^{2}H NMR spectra were calculated from the quadrupolar splittings using the relation (Brown, 1996):

$$|\Delta\nu_Q^{(i)}| = \tfrac{3}{2}\chi_Q|S_{CD}^{(i)}||P_2(\cos\theta)|, \quad (3)$$

where $\chi_Q \equiv (e^2qQ/h) = 167$ kHz (Davis, 1983), θ represents the angle between the bilayer director axis and the static magnetic field direction, and $P_2(\cos\theta) = (3\cos^2\theta - 1)/2$, which, for $\theta = 0°$, is equal to unity. Based on geometrical considerations the values of $S_{CD}^{(i)}$ are assumed to be negative.

DEUTERIUM NMR RESULTS

Disaturated phosphatidylcholines in the liquid-crystalline state

Representative ^{2}H NMR spectra at 50°C are shown in Fig. 1 for a homologous series of disaturated phosphatidylcholines having different acyl lengths. Powder-type ^{2}H NMR spectra of the randomly oriented multilamellar dispersions (fully hydrated; 50 wt % H_2O) are shown at left, and the corresponding deconvoluted (de-Paked) ^{2}H NMR spectra due to the $\theta = 0°$ bilayer orientation are shown at right. Several conclusions can be immediately drawn from the ^{2}H NMR lineshapes in Fig. 1. First, the ^{2}H NMR spectra are indicative of a uniform spherical distribution of the bilayer director axes, and little or no orientation of the bilayers by the relatively high magnetic field strength of 8.48 T is evident. This is supported by the de-Paked ^{2}H NMR spectra at right in Fig. 1, which are of relatively high quality and evince little or no distortion. Second, the ^{2}H NMR spectra are characteristic of axially symmetric motions of the phospholipids about the bilayer normal (director axis), with a distribution of quadrupolar splittings due to the various inequivalent methylene and methyl groups of the perdeuterated acyl chains. Moreover, the *sn*-1 and *sn*-2 acyl groups are inequivalent, as revealed by ^{2}H NMR spectra of multilamellar dispersions of DPPC-d_{62} (both chains perdeuterated) compared to DPPC-d_{31} (*sn*-2 chain deuterated) (spectra not shown). This inequivalence is due to variations in the motional behavior of the individual acyl segments. Finally, the magnitudes of the quadrupolar splittings indicate that the phospholipids possess considerable disorder due to *trans–gauche* rotational isomerizations and other degrees of freedom (see below). The distribution of the quadrupolar splittings is related to the acyl length and cross-sectional area distributions as considered in further detail below.

Of particular interest here is the dependence of the ^{2}H NMR spectra of the homologous phosphatidylcholines on the length of the acyl chains. Both the ^{2}H NMR powder-type spectra (*left*) of the randomly oriented multilamellar dispersions, and the corresponding de-Paked spectra (*right*) show that the quadrupolar splittings increase with increasing chain length. In particular, the de-Paked ^{2}H NMR spectra allow for a better comparison between the lipids due to the increased resolution of the various inequivalent quadrupolar splittings. As a rule, disaturated phosphatidylcholines in the fluid state are distinguished by the Me-2-3-2 spectral pattern present at all temperatures above the melting transition, as can be seen clearly in the de-Paked ^{2}H NMR spectra at right in Fig. 1. Specifically, moving away from the central methyl peak, the quadrupolar splittings fall into groups of 2, 3, and 2 peaks, followed by the larger peaks with the greatest quadrupolar splittings. The latter represent the so-called plateau region because it contains the unresolved splittings corresponding to acyl segments close to the glycerol backbone (beginning of the acyl chain), all of which possess a similar degree of disorder. With increasing acyl length at fixed temperature, the plateau peak becomes larger and it shifts toward larger quadrupolar splittings. This behavior indicates that the length of the plateau acyl chain region increases and becomes less disordered as more mass is added in the hydrocarbon region.

Order profiles: Effect of acyl length

The above observations are more evident upon reduction of the ^{2}H NMR spectral data in terms of order parameter profiles. The spectral assignments and the corresponding quadrupolar splittings for the $\theta = 0°$ orientation, $(\Delta\nu_Q)_\parallel$ obtained as described in the Experimental Methods section, are summarized in Tables 1–4. The order parameters $S_{CD}^{(i)}$, which are model free, are plotted as a function of the acyl segment position in Fig. 2, and provide a quantitative measure of the degree of order along the lipid acyl chains. In each case, the order parameters of the initial segments, close to the glycerol and headgroup region, show a broad plateau followed by a reduction in ordering toward the central region of the bilayer. The characteristic order profile is due to the tethering and alignment of the acyl segments near the aqueous interface, with the increased disorder in the bilayer center due to chain terminations. The order parameters for each lipid decrease with T, reflecting the increased chain disorder resulting from raising the temperature (entropic effect). The largest influence of temperature is on the initial plateau region of the acyl chains, which becomes both more disordered and narrower with increasing T, leading to an overall narrowing of the order profiles.

TABLE 1 De-Paked ^{2}H NMR spectral assignments and $(\Delta\nu_Q)_\parallel$ splittings for DLPC-d_{46} in the liquid-crystalline (L_α) phase

	Acyl Chain		$(\Delta\nu_Q)_\parallel$/kHz			
Peak	*sn*-1	*sn*-2	10°C	30°C	50°C	65°C
A	2–3	3	57.5	48.3	43.8	40.2
B	4	4	57.5	48.3	43.8	39.3
C	5	5	57.5	48.3	40.6	36.2
D	–	6	57.5	46.6	40.6	35.1
E	6	–	57.5	46.6	39.8	35.1
F	–	7	54.3	46.6	39.8	35.1
G	7	8	54.3	42.1	35.8	30.2
H	8	9	51.1	39.0	31.6	27.8
I	9	–	45.0	33.7	27.3	23.0
J	–	10	43.3	31.7	25.2	21.2
K	10	–	39.0	28.9	23.1	19.7
L	–	11	35.5	25.4	19.8	16.5
M	11	–	28.8	21.0	16.6	14.0
N	12	12	8.67	6.07	4.46	3.62

TABLE 3 De-Paked ^{2}H NMR spectral assignments and $(\Delta\nu_Q)_\parallel$ splittings for DPPC-d_{62} in the liquid-crystalline (L_α) phase

	Acyl Chain		$(\Delta\nu_Q)_\parallel$/kHz		
Peak	*sn*-1	*sn*-2	50°C	65°C	80°C
A	2–6	3–6	49.6	45.3	40.8
B	7	7	49.6	42.2	38.0
C	8	8	49.6	42.2	35.5
D	9	9	44.8	37.3	31.8
E	–	10	44.8	34.7	29.2
F	10	11	42.1	34.7	29.2
G	11	12	37.4	30.8	25.5
H	12	13	33.8	28.0	23.1
I	13	–	30.2	24.3	20.2
J	–	14	27.9	22.4	18.2
K	14	–	25.3	20.6	17.1
L	–	15	22.0	17.4	14.2
M	15	–	18.9	15.4	12.7
N	16	16	5.36	4.23	3.52

Further perspective on the order parameter results is gained by comparison of the data for the different lipids at a fixed absolute temperature, as shown in Fig. 3. A first observation is that the plateau regions are larger in magnitude and broader for longer chains. This is basically opposite to the temperature effect described above. However, although the plateau region shows a strong chain-length dependence at any given temperature, the nonplateau segments (chain ends) are practically independent of chain length. This second observation suggests that, at least in a first approximation, the differences in the structure and dynamics of different acyl chain lengths at the same absolute temperature can be obtained just from the analysis of the plateau regions.

One particular goal of the ^{2}H NMR data analysis is to relate the above order parameter profiles to the average projections of the acyl chain segments onto the bilayer normal, with the purpose of calculating the average lipid chain length and the area per lipid in the fluid state. To achieve this goal, one needs to construct a statistical model for the segmental configurations.

THEORY

Segmental motions

The S_{CD} parameters in ^{2}H NMR spectroscopy comprise experimental observables that are measures of the carbon–deuteron (CD) bond orientations with respect to the static external magnetic field axis. Let β_{PL} be the instantaneous angle between the C–D bond and the direction of the static external magnetic field $\mathbf{B_0}$. In terms of the rotation group parameters, β_{PL} is the polar angle (colatitude) of the Euler angles $\Omega_{PL} = (\alpha_{PL}, \beta_{PL}, \gamma_{PL})$ that rotate the quadrupolar coupling tensor from its principal axes system P to the laboratory frame L defined by the magnetic field (see Fig. 4). The quadrupolar splitting $\Delta\nu_Q$ measured by ^{2}H

TABLE 2 De-Paked ^{2}H NMR spectral assignments and $(\Delta\nu_Q)_\parallel$ splittings for DMPC-d_{54} in the liquid-crystalline (L_α) phase

	Acyl Chain		$(\Delta\nu_Q)_\parallel$/kHz		
Peak	*sn*-1	*sn*-2	30°C	50°C	65°C
A	2–4	3–4	53.3	46.2	43.4
B	5–6	5–6	53.3	46.2	41.6
C	7	7	53.3	49.2	38.0
D	–	8	50.9	49.2	35.4
E	8	9	50.9	40.6	35.4
F	9	10	46.3	36.1	31.0
G	10	11	43.4	32.5	28.1
H	11	–	37.5	28.9	24.1
I	–	12	35.9	26.6	22.4
J	12	–	32.0	24.0	20.6
K	–	13	28.7	20.9	17.4
L	13	–	25.3	18.0	15.0
M	14	14	6.83	5.10	4.03

TABLE 4 De-Paked ^{2}H NMR spectral assignments and $(\Delta\nu_Q)_\parallel$ splittings for DSPC-d_{70} in the liquid-crystalline (L_α) phase

	Acyl Chain		$(\Delta\nu_Q)_\parallel$/kHz	
Peak	*sn*-1	*sn*-2	65°C	80°C
A	2–8	3–8	47.1	42.9
B	9	9	43.4	38.0
C	10	10	43.4	34.5
D	11	11	37.9	31.2
E	12	12–13	35.1	29.1
F	13	14	31.7	25.3
G	14	15	28.5	23.0
H	15	–	24.8	20.4
I	–	16	22.5	18.6
J	16	–	21.2	17.4
K	–	17	17.8	14.3
L	17	–	15.8	13.1
M	18	18	4.31	3.65

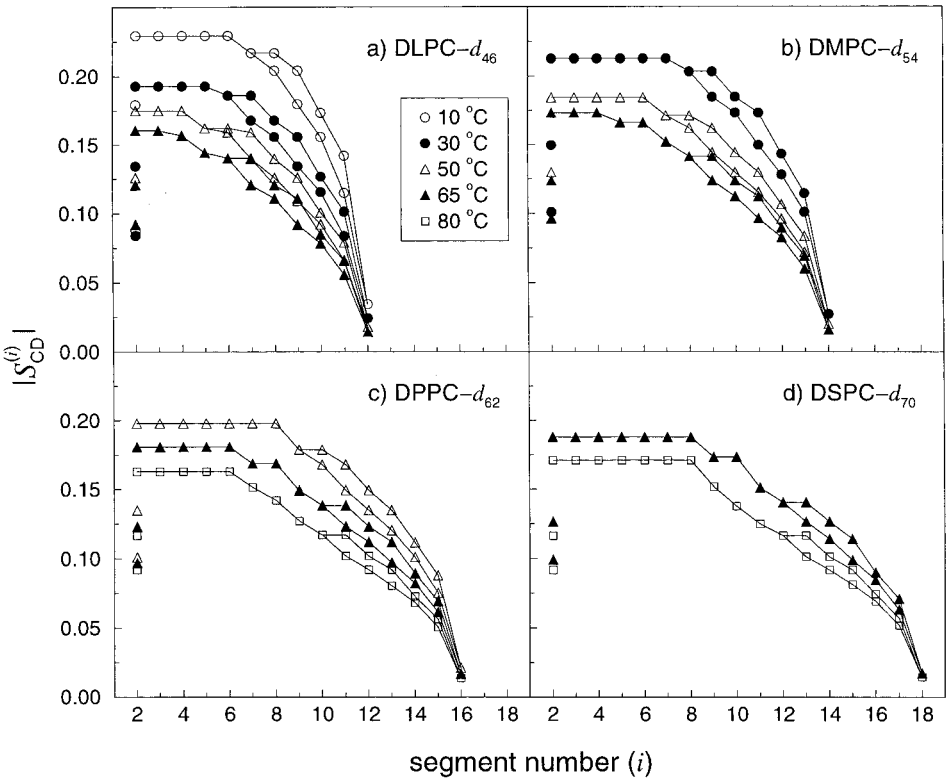

FIGURE 2 (a–d) Measured C–D bond order parameter profiles as a function of carbon number along the acyl chains for the homologous series of disaturated phosphatidylcholines with acyl lengths from $n_C = 12$ to $n_C = 18$. Data for *sn*-1 and *sn*-2 chains are shown separately (but with the same symbols) for each temperature. The double resonances for the C_2 carbon of the *sn*-2 chain are also shown. For each lipid, the order parameters decrease in magnitude with increasing temperature, and the effect is larger for the plateau region.

NMR spectroscopy detects the ensemble average (Brown, 1996)

$$\Delta\nu_Q = \tfrac{3}{2}\chi_Q\langle D_{00}^{(2)}(\Omega_{PL};\, t)\rangle = \tfrac{3}{2}\chi_Q\langle P_2(\cos\beta_{PL};\, t)\rangle. \qquad (4)$$

Here, $\Delta\nu_Q = \nu_Q^+ - \nu_Q^-$, where $\nu_Q^\pm = \nu_\pm - \nu_0$ with ν_0 being the Larmor frequency and $\nu_\pm = \pm(E_{\mp 1} - E_0)/h$ the eigenfrequencies of the single quantum transitions of the $I = 1$ ^{2}H nucleus. Additionally, $\chi_Q \equiv e^2qQ/h$ is the static quadrupolar constant; $D_{00}^{(2)}(\Omega_{PL})$ is the Wigner rotation matrix element with angular momentum $j = 2$ and projections $m = m' = 0$; and P_2 is the second-order Legendre polynomial. The above result is obtained with the assumption that the coupling tensor is axially symmetric (Brown, 1996). The brackets in Eq. 4 indicate an average over the tensor orientations sampled on the NMR time scale, i.e., over the motions that occur on a time scale comparable to, or less than, the inverse quadrupolar splitting. Because of thermal motion, the segmental tensor orientation with respect to the laboratory frame is time dependent, and this fact is indicated in Eq. 4 above.

In principle, one expects the presence of contributions from a hierarchy of motions including segmental motions, molecular motions, and collective fluctuations of the bilayer itself. For the treatment of these various motions, it is convenient to expand the Wigner matrix $D_{00}^{(2)}(\Omega_{PL};\, t)$ in a sequence of frame transformations, using the closure property of the rotation group. In a general formulation, one can write (Brown, 1996),

$$D_{00}^{(2)}(\Omega_{PL};\, t) = \sum_r \sum_q \sum_p \sum_n D_{0r}^{(2)}(\Omega_{PI};\, t) D_{rq}^{(2)}(\Omega_{IM};\, t) \times D_{qp}^{(2)}(\Omega_{MN};\, t) D_{pn}^{(2)}(\Omega_{ND};\, t) D_{n0}^{(2)}(\Omega_{DL}), \qquad (5)$$

where all summations run from -2 to 2. The intermediate frames considered here are the internal frame, I, the molecular axis system, M (not shown in Fig. 4), the local director frame, N, and the average director frame, D. The z axis of the internal frame I is taken to be the normal to the D–C–D plane, and therefore $\beta_{PI} = 90°$. For each chain segment i, this axis gives the orientation of the virtual bond C_{i-1}–C_{i+1}, which we designate as the orientation of segment i. The projection of this virtual bond on the bilayer normal is denoted by D_i. Note that these virtual bond vectors differ from the previous definition of Salmon et al. (1987). Clearly, the expansion of $D_{00}^{(2)}(\Omega_{PL};\, t)$ can include any arbitrary number of coordinate transformations, depending on the motional model considered. The expansion in Eq. 5 is a general example that can be reduced by collapsing those transformations not present in the model (see below).

The C–D order parameter for each chain segment i is defined with respect to the bilayer director frame D, as the ensemble average

$$S_{CD}^{(i)} \equiv \langle D_{00}^{(2)}(\Omega_{PD}^{(i)};\, t)\rangle, \qquad (6)$$

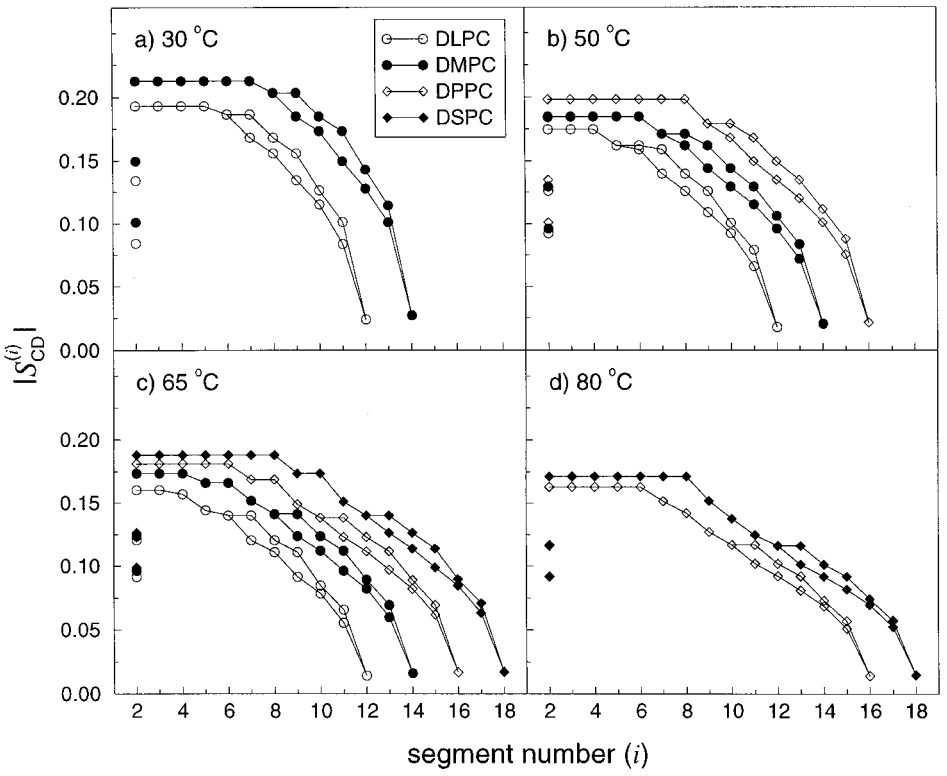

FIGURE 3 (*a–d*) Data as in Fig. 2, plotted at the same absolute temperature in each panel. At any given temperature, the plateau order parameters are larger for longer chains, whereas nonplateau order parameters show little variation.

which, in terms of Eq. 5, includes the first four transformations on the right-hand side. The last Wigner matrix in Eq. 5 describes the fixed transformation from the average director *D*, about which there is cylindrical symmetry, to the laboratory frame *L*, and is accounted for by the de-Pakeing procedure. The above development can be used to relate the spectroscopic observables, viz., the measured C–D bond order parameters, to order parameters that are more convenient to use in describing the structure and dynamics of the acyl chains. How can one compute these ensemble averages? In general, any statistical property $\mathcal{A}(\beta)$ (here β is a generalized Euler angle) can be expressed in terms of a distribution function $f(\beta)$ which gives the ensemble average,

$$\langle \mathcal{A}(\beta) \rangle = \frac{\int_0^{\pi} \mathcal{A}(\beta) f(\beta) \sin \beta \, d\beta}{\int_0^{\pi} f(\beta) \sin \beta \, d\beta}. \qquad (7)$$

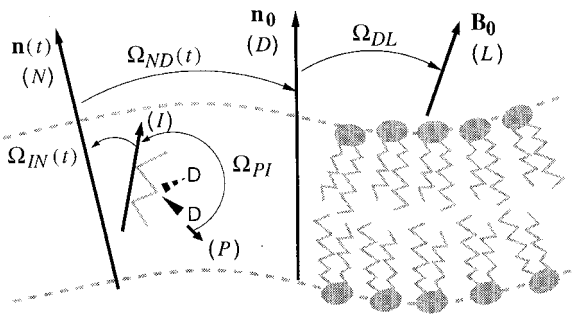

FIGURE 4 Intermediate frames used to describe motions of a D–C–D group in the lipid acyl chains: principal axis system of a C–D bond (*P*), internal frame (*I*), local director frame (*N*), global (average) director frame (*D*), and laboratory frame (*L*). Transformations between frames are carried out by rotations with the Euler angles Ω_{XY}, where *X* and *Y* are generic frame indices. The figure serves for illustrative purposes only and therefore is not drawn to scale.

The orientational distribution function $f(\beta)$ can be expanded in a series of orthogonal polynomials, e.g., the Legendre polynomials $P_j(\cos \beta)$,

$$f(\beta) = \sum_{j=0}^{\infty} \left(\frac{2j+1}{2} \right) \langle P_j(\cos \beta) \rangle P_j(\cos \beta), \qquad (8)$$

where the $\langle P_j(\cos \beta) \rangle$ comprise the various moments of the distribution, i.e., order parameters. Clearly, knowledge of all the moments is required to specify the distribution function. However in many cases only the lower moments are available. In this formulation, the order parameter S_{CD} measured by ^{2}H NMR spectroscopy is related to the second moment $\langle P_2(\cos \beta) \rangle$ of the orientational distribution function $f(\beta)$. As a rule, $f(\beta)$ is a function of both even- and odd-rank order parameters, $\langle P_j(\cos \beta) \rangle$, including of particular interest the odd-rank term $\langle P_1(\cos \beta) \rangle$, which is related

to the acyl chain segmental projection on the bilayer normal. One therefore needs to use a model of segmental conformations to reconstruct $\langle P_1(\cos\beta)\rangle$ given $\langle P_2(\cos\beta)\rangle$. In other words, one needs to assume a functional form for the orientational distribution function $f(\beta)$. The conventional approach, namely the diamond lattice model, is briefly reviewed in the next section, followed by a detailed description of the continuum model developed in this paper.

The diamond lattice model

The diamond lattice model developed by Schindler and Seelig (1975) has been extensively used to model the measured order parameters. Here we give a short derivation in terms of the orientational distribution function, $f(\beta_{IM})$, of the chain segments (virtual bonds) relative to the molecular axis M (Salmon et al., 1987; Jansson et al., 1992; Douliez et al., 1995). In this model, the transformations considered are from the principal axis system P to the internal frame I, then from I to the molecular system M, where M is taken as coincident with the local director frame N (see Eq. 5). The model assumes that the C–D bond orientations fall on a tetrahedral lattice with segment orientations $\beta_i = 0°$, 60°, 90°, 120°, 180°, where the subscript IM has been suppressed for clarity. For such a model of discrete segmental orientations, the moments of the segmental distribution are given by

$$\langle P_j(\cos\beta)\rangle = \sum_i p_i P_j(\cos\beta_i), \tag{9}$$

where the probabilities p_i are normalized ($\Sigma_i p_i = 1$). Evidently, substitution into Eq. 8 gives the distribution function,

$$f(\beta) = \sum_i p_i \sum_{j=0}^{\infty}\left(\frac{2j+1}{2}\right)P_j(\cos\beta_i)P_j(\cos\beta)$$
$$= \sum_i p_i \delta(\beta-\beta_i), \tag{10}$$

where δ denotes the Dirac delta function. By construction of the model, the distribution function $f(\beta)$ is basically a sum of delta functions centered at discrete orientations β_i. As noted above, the average value of any angular dependent quantity can then be obtained as

$$\langle \mathcal{A}(\beta)\rangle = \int_0^{\pi} \mathcal{A}(\beta) f(\beta)\sin\beta\, d\beta = \sum_i p_i \mathcal{A}(\beta_i), \tag{11}$$

where

$$\int_0^{\pi} \mathcal{A}(\beta)\delta(\beta-\beta_i)\sin\beta\, d\beta = \mathcal{A}(\beta_i), \tag{12}$$

and

$$\int_0^{\pi} f(\beta)\sin\beta\, d\beta = 1. \tag{13}$$

In this framework, neglecting the contribution from the orientations at 120° and 180° due to backfolding of the chains (Schindler and Seelig, 1975; Salmon et al., 1987), one obtains for the C–D bond,

$$S_{CD} = p_0 S_{90} + \tfrac{1}{2}p_{60}(S_{35.3} + S_{90}) + p_{90}S_{35.3} = \tfrac{1}{2}(-p_0 + p_{90}), \tag{14}$$

where $S_\beta \equiv \langle p_2(\cos\beta)\rangle$ and

$$\langle D\rangle/D_M = p_0\cos 0° + p_{60}\cos 60° + p_{90}\cos 90°$$
$$= p_0 + \tfrac{1}{2}p_{60}\,. \tag{15}$$

Given that the probability function is normalized ($p_0 + p_{60} + p_{90} \approx 1$), the above are combined to yield Eq. 1 of the Introduction. The acyl chain length in the molecular frame M, relative to the all-*trans* state, is then calculated by summing over all carbon segments (Salmon et al., 1987), giving

$$\frac{\langle L\rangle}{D_M} = \left(\frac{n_C - 1}{2}\right) + \sum_{i=2}^{n_C-1} |S_{CD}^{(i)}| + 3|S_{CD}^{(nC)}|, \tag{16}$$

where the last term of the sum represents the contribution of the terminal methyl. Because the configurational statistics of the segments are only considered with respect to the molecular frame, the above model neglects molecular motions and collective bilayer motions (see below).

The mean-torque model

Using the same framework, one can also consider a continuum model of segmental orientations, which has been shown to be superior to the diamond lattice model result (Petrache et al., 1999; Smondyrev and Berkowitz, 1999). In this model, we retain from Eq. 5 the intermediate frames shown in Fig. 4, namely the internal frame I, the local director frame N, and the average director frame D. Assuming that i) there is cylindrical symmetry about the local director, and ii) the local motions with respect to the local director axis and the director fluctuations are statistically independent, we have that the observed second-rank order parameter is given by

$$S_{CD}^{(i)} = -\tfrac{1}{2}\langle P_2(\cos\beta_{IN}^{(i)}; t)\rangle\,\langle P_2(\cos\beta_{ND}; t)\rangle. \tag{17}$$

The first bracket of the right-hand term in the above expression is the molecular order parameter of the ith segment with respect to the local director $\mathbf{n}(t)$; as such, it combines internal degrees of freedom (chain isomerization) and mo-

lecular motion relative to the local director $\mathbf{n}(t)$. The second bracket in Eq. 17 is the order parameter of the local director itself with respect to the global (average) director, $\mathbf{n}_0$, and describes the order director fluctuations (ODF). Similar to Eq. 17, we can write the corresponding relation for the first-rank order parameters,

$$\langle P_1(\cos \beta_{ID}^{(i)}; t)\rangle = \langle P_1(\cos \beta_{IN}^{(i)}; t)\rangle \langle P_1(\cos \beta_{ND}; t)\rangle. \quad (18)$$

For a statistical treatment of the segmental configurations, we assume that the orientational order for each chain segment i, relative to the local director frame N, can be described by a mean-field orientational potential (potential of mean torque), denoted by $U(\beta_{IN}^{(i)})$. In what follows, we absorb the superscript i and the subscripts IN for clarity, and consider the series expansion of the mean-torque potential $U(\beta)$ in terms of Legendre polynomials,

$$U(\beta) = U_1P_1(\cos \beta) + U_2P_2(\cos \beta) + \cdots. \quad (19)$$

It should be remarked that the above decomposition includes both even and odd parity terms. In particular, the presence of a nonvanishing odd term is a consequence of tethering of the acyl chains, within a given monolayer, to the aqueous interface (Halle, 1991; Trouard et al., 1992). The energy parameters U_1 and U_2 depend upon various factors such as the chain position i, temperature, pressure, and hydration level. Mathematically, U_1 and U_2 are the moments of the function $U(\beta)$ in terms of the Legendre polynomials. Note that $U(\beta)$ completely specifies the distribution function $f(\beta)$, and hence all the moments $\langle P_j(\cos \beta)\rangle$. The functional form of the distribution function is given by the Boltzmann factor, leading to

$$f(\beta) = \frac{1}{Z}\exp\left(-\frac{U(\beta)}{k_BT}\right), \quad (20)$$

with the partition function Z being

$$Z = \int_0^{\pi} \exp\left(-\frac{U(\beta)}{k_BT}\right) \sin \beta \, d\beta. \quad (21)$$

(Note that the orientational potential $U(\beta)$ is defined up to a β-independent additive term, and this fact should be taken into account in free energy calculations.) For convenience of notation, we introduce the following dimensionless parameters:

$$x = \cos \beta, \quad (22)$$

$$\epsilon_1 = -\frac{U_1}{k_BT}, \quad (23)$$

$$\epsilon_2 = -\frac{3U_2}{2k_BT}. \quad (24)$$

Given the orientational preference of the lipid chains, this particular choice for the sign makes ϵ_1 a positive quantity for the upper monolayer, i.e., the chain segments in the upper monolayer have mostly positive projections on the bilayer normal (see Fig. 4). The opposite is true for the lower monolayer, because the two monolayers are related by inversion (Trouard et al., 1994). Using the above notations, we can rewrite Eq. 21 up to second order as

$$Z = \int_{-1}^{1} \exp(\epsilon_1 x + \epsilon_2 x^2)\, dx. \quad (25)$$

It is useful to note the features of the probability distribution generated by $U(x)$ (called the singlet orientational distribution function), namely

$$f(x) = \frac{1}{Z}\exp(\epsilon_1 x + \epsilon_2 x^2), \quad (26)$$

as a function of the mean-torque parameters ϵ_1 and ϵ_2. For the analysis of ^{2}H NMR data, we are interested in the ensemble averages $\langle x\rangle$ and $(3\langle x^2\rangle - 1)/2$, which are precisely the Legendre coefficients (moments) of the orientational distribution $f(x)$. Figure 5 shows semilogarithmic plots of $f(x)$ for an odd-rank parameter $\epsilon_1 = 3$ (a typical value for the lipids considered) and three different values for the even-rank parameter ϵ_2. A positive ϵ_2 increases the probability at $x = \pm 1$ versus $\epsilon_2 = 0$. In particular, the increase around $x = -1$ corresponds to the presence of chain end "upturns" (Nagle, 1993), as measured experimentally by Nuclear Overhauser Effect NMR spectroscopy (Xu and Cafiso, 1986; Huster et al., 1999) and observed in molecular dynamics simulations (Petrache et al., 1999; Feller et al., 1999). Conversely, a negative ϵ_2 gives rise to a maximum of $f(x)$, as shown in Fig. 5, that shifts from $x = 1$ toward $x = 0$ as the absolute magnitude of ϵ_2 increases (not

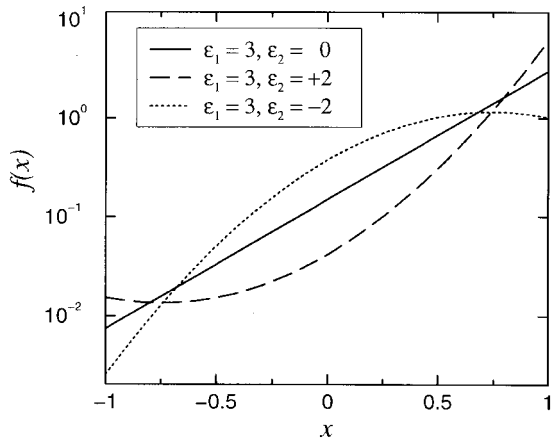

FIGURE 5 Semilogarithmic plots of orientational distribution $f(x)$ of the chain segment tilt $x \equiv \cos \beta$. Results are shown for an odd-rank parameter of $\epsilon_1 = 3$ and even-rank parameter of $\epsilon_2 = -2$, 0, and 2. The $\epsilon_2 > 0$ case models upturns, whereas $\epsilon_2 < 0$ models the case when the point of maximum probability shifts away from $x = 1$.

shown). This models the situation when the most probable segment orientation is tilted (i.e., $x \neq 1$) relative to the local z-axis. We emphasize that one should make a distinction between the most probable tilt and the average tilt $\langle x \rangle$, the latter being generally smaller in magnitude than the former (see Pastor et al., 1988, 1990, on lipid "wobbling" motion). This fact is a direct consequence of the strong asymmetry of $f(x)$ about $\langle x \rangle$, and, as we show later, it plays a major role in the calculation of the area per lipid.

For a complete description of the orientational potential $U(x)$, one would like to determine the mean-torque parameters ϵ_1, ϵ_2, . . . , from which thermodynamic quantities can be calculated. Equivalently, the orientational distribution function $f(x)$ can be completely reconstituted if one knows all its moments

$$\langle x^k \rangle = \frac{1}{Z} \int_{-1}^{1} x^k f(x)\, dx, \quad k = 1,2, \ldots . \tag{27}$$

In practice, the ^{2}H NMR observables give only the second-rank moment $\langle x^2 \rangle$, via its relationship with the S_{CD} order parameter,

$$\langle x^2 \rangle = \frac{1 - 4S_{CD}}{3}, \tag{28}$$

which is obtained from Eq. 17 assuming a negligible contribution from order director fluctuations. With only one available constraint, i.e., the value of $\langle x^2 \rangle$, the two parameters, ϵ_1 and ϵ_2, cannot be determined independently; rather, one finds a set of solutions in the (ϵ_1, ϵ_2) plane. Such solutions, obtained numerically, using Eqs. 25–28, are presented in Fig. 6 *a* for S_{CD} values within the experimental range.

For the analysis of the acyl chain average structure, we seek to determine the average segment projection $\langle x \rangle$, i.e., the first moment of $f(x)$, given the second moment $\langle x^2 \rangle$, for all segments along the chain (Jansson et al., 1992). As found in molecular dynamics simulations (Petrache et al., 1999), the distributions $f(x)$ are all reasonably well modeled by simple exponential functions, meaning that the ϵ_1 term is the dominant term. We can therefore consider that, in general, $|\epsilon_2| < \epsilon_1$, which is especially true for the plateau segments, which are closer to the water interface and therefore feel a stronger restoring potential. The excluded region $|\epsilon_2| > \epsilon_1$ is indicated in Fig. 6 by the gray area. The solutions in Fig. 6 *a* correspond to the quantity of interest, namely $\langle x \rangle$, which is shown in Fig. 6 *b* as a function of ϵ_2 for the given values of S_{CD}. Again, the figure emphasizes the allowed region $|\epsilon_2| < \epsilon_1$. We observe that, for large values of S_{CD} corresponding to the plateau region in the ^{2}H NMR profiles, the first moment $\langle x \rangle$ is almost insensitive to ϵ_2, as revealed by the plateau regions of $\langle x \rangle$ in the vicinity of $\epsilon_2 = 0$. This is an important aspect, because it justifies the use of an $\epsilon_2 = 0$ model for the treatment of plateau carbons. Therefore, as a first approximation, we can set $\epsilon_2 = 0$ when S_{CD} is safely large, and, in this way, eliminate one unknown variable. The only unknown variable left is ϵ_1, which can now be uniquely determined for each given S_{CD} by solving Eqs. 25–28 self-consistently (intersection of the constant S_{CD} curves in Fig. 6 *a* with the vertical dashed line at $\epsilon_2 = 0$). We will call this the first-order mean-torque model (MT), because it only involves the first term in the Legendre expansion of the mean-torque potential (Eq. 19). In the framework of this model, from each measured $S_{CD}^{(i)}$, one finds the corresponding mean-torque parameter $\epsilon_1^{(i)}$, assuming that $\epsilon_2^{(i)} = 0$. The average chain projections $\langle x^{(i)} \rangle$ are then calculated using the values of $\epsilon_1^{(i)}$ obtained in this way. Note that we have reintroduced the chain segment index i to emphasize that the mean-torque parameter $\epsilon_1^{(i)}$ depends on chain position.

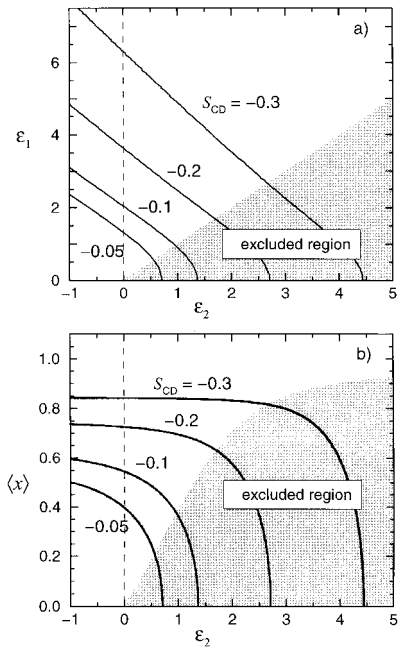

FIGURE 6 (*a*) Curves of constant S_{CD} in the (ϵ_1, ϵ_2) plane, obtained by solving Eq. 27 for $k = 1$ and $k = 2$ self-consistently. (*b*) Dependence of $\langle x \rangle$ on ϵ_2 for given values of S_{CD}. Because the acyl chains are tethered to the water interface, the ϵ_1 term in the orientational distribution function $f(x)$ is dominant, especially for the initial segments (plateau). In consequence, the region $\epsilon_2 > \epsilon_1$ is excluded as explained in the text. Part (*b*) shows that, for large enough $|S_{CD}|$ values (plateau region), the value of $\langle x \rangle$ is practically independent of ϵ_2.

The first-order mean-torque model

Basically, this is the model proposed by Petrache et al. (1999) for the analysis of simulated order parameter profiles. Given the second moment $\langle x^2 \rangle$ (or equivalently S_{CD}), the first moment $\langle x \rangle$ is calculated by numerically solving the following coupled equations [see Eqs. 17 and 18 in Petrache

et al. (1999)]:

$$\langle x\rangle = \frac{1}{Z}\int_{-1}^{1} x e^{\epsilon_1 x}\,dx = \coth(\epsilon_1) - \frac{1}{\epsilon_1}, \qquad (29)$$

$$\langle x^2\rangle = \frac{1}{Z}\int_{-1}^{1} x^2 e^{\epsilon_1 x}\,dx = 1 + \frac{2}{\epsilon_1^2} - \frac{2}{\epsilon_1}\coth(\epsilon_1). \qquad (30)$$

Figure 7 *a* shows the numerical results of $\langle x\rangle$ versus $\langle x^2\rangle$ for the first-order MT that was obtained by eliminating ϵ_1 between Eqs. 29 and 30. Figure 7 *a* emphasizes that the variance

$$\sigma^2 = \langle x^2\rangle - \langle x\rangle^2 \approx 1/\epsilon_1^2, \qquad (31)$$

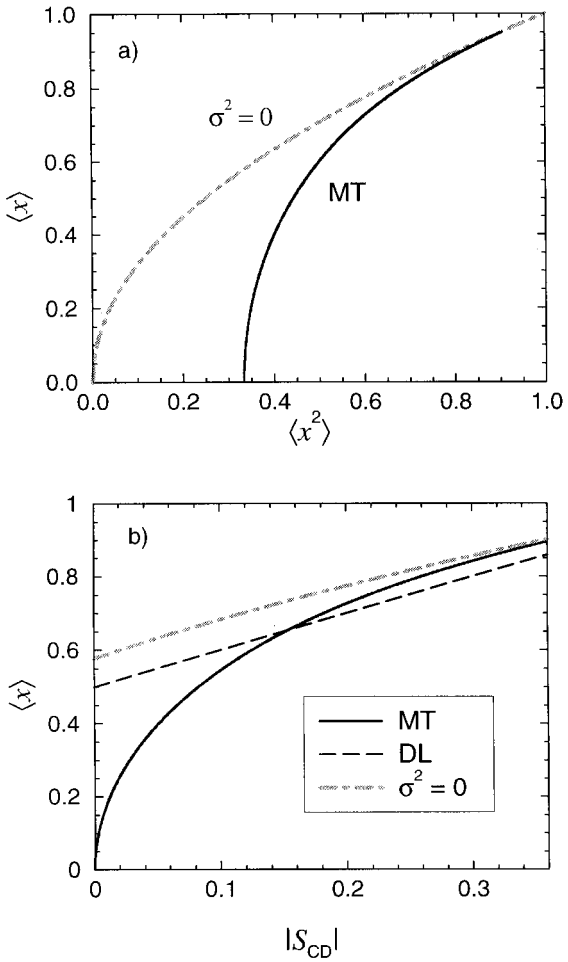

FIGURE 7 (*a*) *Solid line,* numerical result from Eqs. 29 and 30 for first moment, $\langle x\rangle$, of $f(x)$ as a function of second moment, $\langle x^2\rangle$, given by the first-order MT; *dot-dashed line,* the function $\langle x\rangle = \sqrt{\langle x^2\rangle}$ shown for comparison (the case of variance $\sigma^2 = 0$). (*b*) *Solid line,* $\langle x\rangle$ versus $|S_{CD}|$ obtained by solving Eqs. 29 and 30 numerically; *dot-dashed line,* the function $\langle x\rangle = \sqrt{\langle x^2\rangle}$ (case of $\sigma^2 = 0$); *dashed line,* DL result.

of $f(x)$ is significant. If $f(x)$ were a delta function, then the variance σ^2 would vanish, and give $\langle x\rangle = \sqrt{\langle x^2\rangle} = x$. This limiting case is shown in Fig. 7 *a* with the dot-dashed line for comparison with the more realistic $\sigma^2 \neq 0$ case. The first-order mean-torque result for $\langle x\rangle$ is shown again in Fig. 7 *b*, but this time as a function of the measured order parameters S_{CD}. The utility of this second plot is that it can be used to convert the measured S_{CD} into the average segmental projection $\langle x\rangle$, as described below. Note however that, for small order parameters (chain ends), the calculated S_{CD} is an overestimate, resulting from the neglect of ϵ_2 in the potential of the mean-torque. For large $|S_{CD}|$ values, the MT gives higher values of $\langle x\rangle$ than the diamond lattice model (DL), which is shown for comparison. For $|S_{CD}^{(i)}| > 1/8$, which is in the range of most ^{2}H NMR plateau values for lipid membranes, an analytical solution for $\langle x\rangle$ can be obtained, as shown by Petrache et al. (1999). This analytical solution is obtained from Eqs. 29 and 30 by making the approximation $\coth(\epsilon_1) \approx 1$, giving

$$\langle x^{(i)}\rangle = 1 - \frac{1}{\epsilon_1^{(i)}}, \qquad (32)$$

with

$$\epsilon_1^{(i)} = \frac{2}{1 - \sqrt{(-8S_{CD}^{(i)} - 1)/3}}. \qquad (33)$$

Note that, by eliminating the mean-torque parameter $\epsilon_1^{(i)}$ in the above equations, we recover Eq. 2 of the Introduction. Typical values for the dimensionless parameter ϵ_1 corresponding to the plateau segments, are between 2.5 and 6, as can be seen from Fig. 6 *a* for $\epsilon_2 = 0$. For the plateau order parameters of DPPC-d_{62} at 50°C, ϵ_1 is roughly 3.5, which corresponds to a mean-torque potential $|U_1| = k_B T\epsilon_1$ of about 9.6 kJ/mol. Similar to the diamond lattice approach, by letting $\epsilon_1^{(i)}$ vary along the chain, one can estimate the average projection $\langle x^{(i)}\rangle$ for each carbon, using the corresponding order parameter $S_{CD}^{(i)}$.

Slow motions: Order director fluctuations

Both the DL and the MT as presented above neglect the possible contributions from slower bilayer motions (Brown, 1982, 1996). In particular, for the case of a DL, one needs to consider the contribution from noncollective molecular motions, as well as collective motions, e.g., ODF. The latter motion (ODF) should be considered in both the DL and MT. These contributions can be treated with the assumption of time-scale separation between the fast local segmental motions and slow motions of collective or noncollective origin. However, we note that this decomposition can be made for any uncorrelated motions, regardless of time scales. With this assumption, the measured order parameters are then

given by

$$S_{CD}^{(i)} = S_{fast}^{(i)} S_{slow} = S_{fast}^{(i)} \langle P_2(\cos \beta_{XD}; t) \rangle, \quad (34)$$

where $S_{fast}^{(i)}$ denotes segmental order parameters that depend on the segment index i (as considered in DL and MT above), and S_{slow} represents the contribution from additional motions that are assumed to be independent of segment position. The generalized frame index X stands for either the molecular frame M or the local director frame N. Similarly, the average chain length relative to the average bilayer normal (director axis) is given by

$$\langle L \rangle = \langle L \rangle_{fast} \langle P_1(\cos \beta_{XD}; t) \rangle. \quad (35)$$

To proceed further, one needs a tractable model of slow motions. For example, one possibility is to treat the contribution from ODF by assuming that the local director $\mathbf{n}(t)$ moves in a cone about the global director $\mathbf{n_0}$. In this model (Jansson et al., 1992), we have that

$$\langle P_1 \rangle_{slow} = \tfrac{1}{2}(1 + \cos \beta_c), \quad (36)$$

and

$$\langle P_2 \rangle_{slow} = \tfrac{1}{2} \cos \beta_c (1 + \cos \beta_c), \quad (37)$$

where β_c is a model parameter and represents the cone semi-angle. Eliminating $\cos \beta_c$ between the last two equations above, we obtain for the projected acyl chain length,

$$\langle L \rangle = \frac{1 + \sqrt{1 + 8S_{slow}}}{4} \langle L \rangle_{fast}, \quad (38)$$

which is a usual correction used for the analysis of order parameters (Douliez et al., 1995).

As an alternative, we can use a mean-torque approach, in analogy with the treatment of fast motions. By isomorphism with the first-order mean-torque result in Eq. 2, we then have

$$\langle L \rangle = \frac{1}{2} \left(1 + \sqrt{\frac{4S_{slow} - 1}{3}} \right) \langle L \rangle_{fast}. \quad (39)$$

It has been argued however that S_{slow} does not change the value of $\langle L \rangle$ significantly for typical lipids in the fluid lamellar state (Brown, 1996). The reason is that the slow motion correction increases the estimate for the chain projection $\langle L \rangle_{fast}$ in a first stage (because $S_{fast} = S_{CD}/S_{slow} > S_{CD}$), but then the effect is reduced when the prefactor $\langle P_1 \rangle_{slow}$ is considered in the final expression for $\langle L \rangle$. For instance, assuming a value of $S_{slow} = 0.7$ increases the final predicted $\langle L \rangle$ by only 1.5%. It follows that such relatively slow bilayer motions are mainly important for consideration of the bilayer dynamics, i.e., the rates of the structural fluctuations. Because the slow motion correction to the calculated values of $\langle A \rangle$ is most likely small, and because the precise value of S_{slow} may have a subtle dependence on temperature and chain length, we shall work in the approximation that $S_{slow} = 1$. We note however that using FTIR measurements in combination with ^{2}H NMR spectroscopy, one can (in principle) dissociate *trans–gauche* isomerization from other molecular motions (Davies et al., 1992; Tuchtenhagen et al., 1994) to give an estimate for the slow order parameter S_{slow}.

Calculation of the area per lipid

For the planar lamellar phase, the hydrophobic thickness and the area per lipid are the two most relevant structural parameters. Due to thermal motion, especially in the fluid state, the individual lipids adopt a wide variety of instantaneous molecular shapes, so therefore a proper definition of the area per lipid $\langle A \rangle$ necessarily involves some sort of ensemble averaging. This calculation (averaging) requires a statistical mechanical model for the local segmental fluctuations, such as those described above. Regardless of the model used, one faces at least two possible alternatives for calculations of $\langle A \rangle$ (Thurmond et al., 1991). The most common treatment is to consider that the chain length and area fluctuations are uncorrelated, and calculate $\langle A \rangle$ using an estimate for the entire acyl chain length. An alternative (Thurmond et al., 1991; Nagle, 1993) is to use just the initial chain segments corresponding to the plateau region. One advantage of this second method is that it avoids the problem of monolayer interdigitation.

For the plateau region, assuming that the segment cross-sectional area and the projected length are inversely correlated (Jansson et al., 1992; Brown, 1996; Petrache, 1999), i.e., for a rectangular or cylindrical cell shape, one has that

$$\langle A \rangle = 4V_{CH_2} \left\langle \frac{1}{D} \right\rangle, \quad (40)$$

which can be rewritten as

$$\langle A \rangle = qA_M, \quad (41)$$

with $A_M = 4V_{CH_2}/D_M$ being the lipid cross-sectional area of the extended all-*trans* chain conformation, and $q \equiv \langle 1/x \rangle$ the area factor. Here, V_{CH_2} denotes the volume of a methylene group, and, as before, D is the instantaneous travel of an individual segment along the bilayer normal, with a maximum value of $D_M = 2.54$ Å.

There has been a long debate regarding the proper way of estimating the average $\langle 1/x \rangle$ (Jansson et al., 1992; Nagle, 1993; Brown, 1996; Petrache et al., 1999). The most straightforward approximation $\langle 1/x \rangle \approx 1/\langle x \rangle$ seems sufficient in some cases, but clearly ignores the width of the distribution $f(x)$, as described by the variance $\sigma^2 = \langle x^2 \rangle - \langle x \rangle^2$. A harmonic approximation about $\langle x \rangle$, namely $\langle 1/x \rangle \approx \langle x^2 \rangle / \langle x \rangle^3$ as proposed recently, although working well for a particular MD data set, fails when applied to experimental data (Petrache et al., 1999). Specifically, for DMPC at

30°C, it gives areas that are too large compared to the currently accepted values (Koenig et al., 1997; Petrache et al., 1998a). The difficulty in estimating $\langle 1/x \rangle$ originates from the misbehavior of $1/x$ at small values of x, with a singularity at $x = 0$. In fact, there are two main conceptual issues regarding the definition of the average area per lipid as given by Eq. 40. First, one is concerned whether the actual area per lipid is properly defined as being proportional to $1/D$ for all values of D. In particular, as D becomes smaller (it can even be zero!), it eventually underestimates the geometrical projection of the CH_2 group as a whole on the z-axis, and, in consequence, overestimates the contribution of these highly tilted groups to the average area. At some point, Eq. 40 breaks down due to the singularity. The second important question is whether the area per lipid can be accurately calculated from the singlet distribution $f(x)$, as opposed to a multiplet distribution that would take into account correlations between neighboring chains. Because these multiplet distributions are not yet incorporated in the current mean field model, we have looked for a satisfactory approximation based on the singlet probabilities $f(x)$ considered above.

These probability distributions, being roughly exponential, are anharmonic and highly asymmetric about the average $\langle x \rangle$. In particular, the largest contribution is given by the values in the vicinity of the point of maximum probability at $x = 1$. Expanding to second order about this point, we obtain

$$q = \left\langle \frac{1}{x} \right\rangle \approx \langle 1 + (1 - x) + (1 - x)^2 \rangle$$

$$= 3 - 3\langle x \rangle + \langle x^2 \rangle. \quad (42)$$

With both the first moment $\langle x \rangle$ and the second moment $\langle x^2 \rangle$ calculated from the C–D order parameters, the area factor q is determined, and then used in Eq. 41 to calculate the average area per lipid $\langle A \rangle$. Having the average area determined, the average hydrocarbon thickness per monolayer is, by definition, calculated as

$$D_C = \frac{2V_C}{\langle A \rangle} = \frac{2V_C}{qA_M}, \quad (43)$$

where V_C is the hydrocarbon chain volume. With the notation n_C for the number of carbons per chain (e.g., 16 for DPPC) and the well-established assumption that the methyl volume is twice the methylene volume, $V_{CH_3} \approx 2V_{CH_2}$ (Nagle and Wilkinson, 1978; Petrache et al., 1997; Armen et al., 1998), the hydrocarbon thickness can be expressed as

$$D_C = \frac{n_C D_M}{2q}. \quad (44)$$

Note that, although the exact value of the area per lipid $\langle A \rangle$ is sensitive to the specific volume measurement, the hydrocarbon thickness D_C, as given by Eq. 44, is a function of the area factor q only, and therefore it is sensitive to the NMR measurement alone.

STRUCTURAL RESULTS

The calculation of the area per lipid requires information on the methylenic volume V_{CH_2} as a function of temperature. Accurate specific volume measurements of lipids have been reported by Nagle and Wilkinson (1978); however, these do not involve direct measurements of V_{CH_2}. Instead, in a typical dilatometry measurement, the lipid molecular volume V_L is determined as a whole. One then needs additional information about the headgroup volume V_H to subtract from V_L to determine the hydrocarbon volume V_C. Initial estimates of V_H (which includes the phosphocholine, the glycerol backbone, and the carbonyl groups) gave values of about 340 Å^3 (Nagle and Wiener, 1988) based on gel state data. More recent analysis of DPPC gel state data yields that $V_H = 319$ Å^3 (Sun et al., 1994). Additional information regarding lipid component volumes is provided by molecular dynamics simulations (Petrache et al., 1997; Armen et al., 1998). Within the uncertainty of the headgroup volume V_H, the available data suggest that the volume V_{CH_2} for all disaturated lipids in the fluid state is nearly the same as a function of absolute temperature T. Putting together all the available volumetric data, we obtain the empirical relationship, $V_{CH_2}(T) \approx V^0_{CH_2} + \alpha_{CH_2}(T - 273.15\,\text{K})$, where $V^0_{CH_2} = 26.5$ Å^3, and $\alpha_{CH_2} = 0.0325$ Å^3/K. We note, however, that specific volume measurements (Nagle and Wilkinson, 1978) show a certain degree of nonlinearity for DMPC, as opposed to DPPC. These differences should eventually be taken into account when more information on the behavior of the headgroup volume V_H with temperature is available. For the purpose of the current analysis, however, this distinction between the thermal behavior of V_{CH_2} among the different lipids is not necessary.

We have used the measured ^{2}H NMR order parameters (see Tables 1–4) to calculate the hydrocarbon thickness D_C and the area per lipid $\langle A \rangle$ as a function of temperature for the homologous series of 1,2-diacyl-*sn*-glycero-3-phosphocholines with perdeuterated acyl chains. Both the diamond lattice and mean-torque results are shown in Fig. 8 for comparison to emphasize model-independent features. The conventional method using the diamond lattice result and the whole order profile (Eq. 16) is denoted by DL1. The alternate approach uses the diamond lattice expression (Eq. 1) for the plateau region, together with the assumption of uncorrelated area and segmental projection, and is denoted by DL2. Finally, the mean-torque result, based on the calculation of the area factor q using Eq. 42 for the plateau order parameters is denoted by MT. The results for DL1 and DL2 are compared in Fig. 8, *a* and *b*. The first-order MT results are shown in Fig. 8, *b* and *d*, and are also listed in Table 5. In addition, Table 5 gives results for DPPE for comparison (Thurmond et al., 1991).

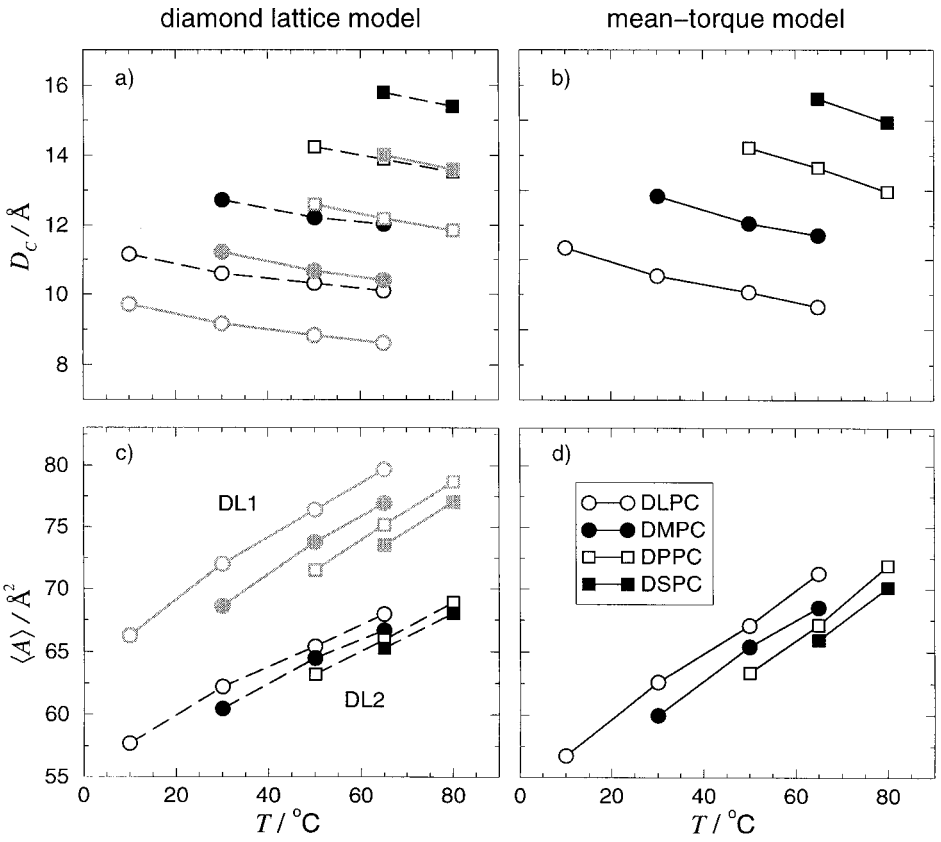

FIGURE 8 Model results for hydrophobic thickness D_C and area per lipid $\langle A \rangle$. (*a, c*) Results from the two diamond lattice methods: full chain (DL1) versus plateau segments (DL2). (*b, d*) Results from the first-order MT using the plateau order parameters only.

As documented by previous studies (Thurmond et al., 1991; Nagle, 1993; Koenig et al., 1997) DL1 gives lower values of D_C and larger values of $\langle A \rangle$ than does DL2. Interestingly, the results from MT and DL2 are similar in magnitude, on average, but their temperature variation is different. More important than the differences among the various treatments, however, Fig. 8 reveals a number of interesting model-independent features of the lipid structural parameters. First, as expected, the hydrocarbon thickness for each lipid decreases and the area increases with increasing temperature. Second, and more interestingly, at any given temperature, lipids with longer chains (higher n_C)

TABLE 5 Summary of structural results for disaturated lipids in the liquid-crystalline (L_α) state

Lipid	T (°C)	S_p	q	D_C (Å)	$\langle A \rangle$ (Å^2)	$\alpha_\parallel$ (10^{-3} K^{-1})	$\alpha_\perp$ (10^{-3} K^{-1})	$\nu_\parallel$ (10^{-2})	$\nu_\perp$ (10^{-2})	L_C^* (Å)	L_C (Å)
DLPC	10	0.229	1.35	11.4	56.7	−3.6	4.8	—	—	9.2	10.9
	30	0.193	1.45	10.5	62.6	−3.9	5.1	10.9	−2.5	8.4	9.9
	50	0.175	1.52	10.1	67.1	−2.3	3.5	9.8	−1.5	7.8	9.2
	65	0.160	1.59	9.6	71.2	−2.9	4.1	10.7	−2.3	7.4	8.7
DMPC	30	0.213	1.39	12.8	60.0	−3.1	4.3	8.9	−1.8	10.6	12.2
	50	0.184	1.48	12.0	65.4	−3.3	4.4	8.2	−1.1	9.7	11.2
	65	0.173	1.53	11.7	68.5	−2.0	3.1	8.8	−1.6	9.3	10.6
DPPC	50	0.198	1.44	14.2	63.3	−2.7	3.8	7.6	−1.4	11.8	13.3
	65	0.181	1.50	13.6	67.1	−2.8	3.9	7.1	−0.9	11.1	12.4
	80	0.163	1.57	13.0	71.9	−3.5	4.6	7.7	−1.4	10.4	11.6
DSPC	65	0.188	1.47	15.6	66.0	−2.9	4.0	6.3	−0.8	13.0	14.3
	80	0.171	1.54	14.9	70.1	−3.0	4.1	6.6	−1.1	12.2	13.5
DPPE	69	0.232	1.34	15.2	60.5	−2.7	3.9	—	—	12.7	14.3
	85	0.209	1.40	14.5	64.4	−2.9	4.0	—	—	12.1	13.5

S_p denotes the plateau order parameter values used to calculate the area factor q (Eq. 42), the hydrocarbon thickness D_C (Eq. 44), and the average area per lipid $\langle A \rangle$ (Eq. 42) using MT. The average chain lengths are calculated using Eq. 45 for L_C^* and Eq. 46 for L_C.

have larger D_C and lower $\langle A \rangle$. These observations are addressed in more detail in the Discussion section.

Besides the hydrocarbon thickness D_C and the area per lipid $\langle A \rangle$, we have also estimated the average chain length L_C (projected on the bilayer normal) using the first-order MT. This projected chain length is not necessarily the same as the hydrocarbon thickness D_C, inasmuch as the degree of interdigitation between the opposing lipid monolayers controls the relationship between L_C and D_C (Nagle, 1993). As mentioned in the Theory section, the use of the linear MT is justified mainly for large S_{CD} values (as in the plateau region). However, for the purpose of comparing data for lipids with different acyl chain lengths, we use it for the nonplateau carbons also, keeping in mind that systematic deviations are included in the results. Using the conversion plot between S_{CD} and $\langle x \rangle$ given in Fig. 7 *b*, we have calculated chain extensions as a function of temperature for the MT. Table 5 shows the results for the chain extent L_C^*, defined as

$$L_C^* = \langle z_2 \rangle - \langle z_{n_C} \rangle = \sum_{i=3,5,\ldots}^{n_C-1} \langle D_i \rangle , \qquad (45)$$

and calculated as a sum over odd carbon projections. Table 5 also gives the results for the conventional chain length L_C (which accounts for the chain extent beyond the end carbons C_2 and C_{n_C}), calculated as

$$L_C = \frac{1}{2} \sum_{i=2}^{n_C-1} \langle D_i \rangle + \langle D_{n_C-1} \rangle . \qquad (46)$$

As expected, the projected acyl length becomes shorter with increasing temperature, as shown in Table 5. Both L_C^* and L_C have been considered by Petrache et al. (1999) in relation with the hydrocarbon thickness D_C, obtained from molecular dynamics simulations. It was found for that particular simulation that the results for L_C and D_C coincided. In contrast, the results presented in Table 5 show that, for the ^{2}H NMR data, both L_C^* and L_C are underestimates of the hydrocarbon thickness D_C (Nagle, 1993).

It is noteworthy that our MT results for the area per lipid are within 1 Å^2 from the corresponding X-ray data for DPPC and DMPC in the fluid state. For DPPC at 50°C, we obtain 63.3 Å^2 as compared to 62.9 Å^2 (Nagle et al., 1996). Similarly, for DMPC at 30°C we obtain an area of 60.0 Å^2 in good agreement with the two most recent measurements of 59.5 Å^2 (Koenig et al., 1997) and 59.7 Å^2 (Petrache et al., 1998a). These MT results are plotted in Fig. 9 *a*, together with the results using the DL. It is interesting to note that the MT and DL2 results are practically the same. This is because the inverse area factor $\langle 1/x \rangle^{-1}$ from MT coincides with the conventional diamond lattice expression $\frac{1}{2} + |S_{CD}|$ in the vicinity of $S_{CD} = 0.2$, as shown in Fig. 9 *b*. In contrast, DL1 overestimates the area due to the underestimation of the hydrocarbon thickness. For DL1 to work properly, one needs to find the right correction to add to the chain length L_C (or L_C^*) to reproduce the hydrocarbon thickness D_C. This correction depends on temperature and possibly other factors. In particular, our current results (Table 5) show an increase of $D_C - L_C^*$ with temperature. This implies a broadening of the methyl end distribution along the membrane normal with increasing temperature for a given chain length (Mely et al., 1975), which is also consistent with the narrowing of the order parameter plateau region.

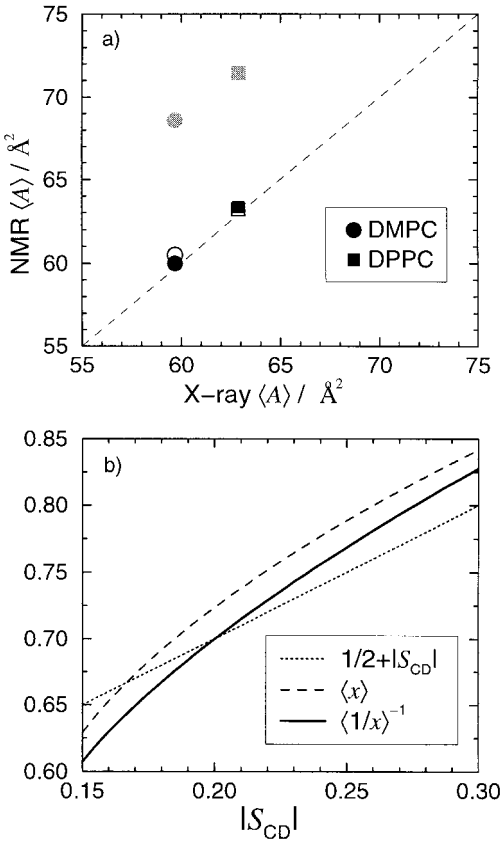

FIGURE 9 (*a*) Lipid area from NMR using DL (*grey symbols,* DL1; *open symbols,* DL2) and MT (*solid symbols*) versus X-ray determined area for DMPC at 30°C and DPPC at 50°C. (*b*) Comparison between DL and MT in terms of predicted $\langle x \rangle$ dependence on $|S_{CD}|$. For larger values of $|S_{CD}|$, the DL (*dotted line*) underestimates $\langle x \rangle$ (*dashed line*), but coincides with the inverse area factor $\langle 1/x \rangle^{-1}$ (*solid line*) in the vicinity of $|S_{CD}| = 0.2$, explaining the agreement between DL2 and MT in part (*a*).

DISCUSSION

General aspects of lipid bilayer structure

At the basic level, membrane structural properties are governed by the forces that drive and stabilize the self-assembly of amphiphilic systems. This force balance is manifested in various aspects of the lipid bilayer microstructure, and it is specifically reflected in the C–D bond order parameters

measured by ^{2}H NMR spectroscopy. The profiles of the order parameters $S_{CD}^{(i)}$ (as shown in Figs. 2 and 3) provide a quantitative measure of the orientational ordering of the lipid acyl chains in the liquid-crystalline (L_α) state. These profiles consist of a plateau in the $S_{CD}^{(i)}$ values over the first part of the chains, followed by a decrease in magnitude toward the chain terminal methyl group. The order gradient reflects a progressive loss of the regularity in chain packing from the aqueous interface toward the bilayer center. In particular, the order parameter for the terminal methyl segment approaches the isotropic limiting value of $S_{CD}^{(i)} \approx 0$, characteristic of an oil drop model. By contrast, the plateau values are significantly larger. A useful comparison is provided by the "crankshaft" model (a polymethylene chain saturated with kinks), which gives an average order parameter of $S_{CD} = -1/3$ (Brown, 1996). Thus, the acyl chains in the lipid bilayer exist in a state of intermediate order, between the limiting crankshaft and oil drop models.

An important issue has then been how to obtain accurate structural parameters for fluid phospholipids in relation to the balance of forces governing the self assembly of amphiphilic systems. The interpretation of the ^{2}H NMR order parameters of phospholipid bilayers has primarily involved lattice models. Alternatives to lattice models, however, have also been considered in the form of numerical calculations based on a phenomenological set of interactions between membrane components (Marčelja, 1974; Meraldi and Schlitter, 1981; Fattal and Ben-Shaul, 1995), with adjustable parameters to match the experimentally measured S_{CD} values. Numerical approaches have also included computer simulations, both in the form of Monte Carlo (Scott, 1986; Chiu et al., 1999) and molecular dynamics (Pastor et al., 1988, 1990). The advantage of computer simulations is that one has a detailed description of the system, and therefore all properties are accessible in principle. Apart from the amount of computing power required for such calculations, and a relative uncertainty in the simulation force-fields, a disadvantage is that physical insight and generality can become obscured. Fortunately, both can be recovered by combining theoretical aspects with the details revealed by the simulations. For the analysis of NMR data, simple (mathematical closed form) relationships between the order parameters and the bilayer thermodynamic properties are desirable. This aspect has motivated recent effort toward combining theory and simulations (Berger et al., 1997; Petrache et al., 1999; Smondyrev and Berkowitz, 1999).

In particular, Petrache et al. (1999) proposed a continuum model of segmental orientations as a better alternative to the DL. Here we consider a mean-field approach for the interpretation of the order parameters, and this methodology puts the order parameter analysis in a more unified framework with the relaxation data analysis (Brown, 1996). We have shown that the continuum segmental distribution can be regarded as a combination of internal degrees of freedom (chain isomerization) and chain motion as a whole, and it is generated by the mean-torque potential felt by each individual chain segment. Using a first-order approximation of the mean-torque potential, we have calculated bilayer structural parameters for fluid disaturated phosphatidylcholines as a function of temperature and chain length. By construction, the model is inherently one-dimensional. The full three-dimensional chain packing is basically reduced to a one-dimensional problem through introduction of the segmental volume V_{CH_2} using Eq. 40, and this expression actually defines the area per lipid molecule. In this sense, the approach is similar to the use of one-dimensional electron density profiles from X-ray experiments, in which the area per lipid is calculated using the distance between the headgroup peaks along the bilayer normal, and the lipid volume V_L (McIntosh and Simon, 1986; Nagle et al., 1996; Petrache et al., 1998a; Tristram-Nagle et al., 1998).

Further correspondence between the NMR and the X-ray approaches resides in the effect of collective bilayer motions (order director fluctuations; Brown, 1982) on the calculated area per lipid. Depending on the amplitude of ODF, one has to distinguish between the local and the projected lipid cross-sectional area. Because of bilayer undulations, even from X-ray data the determination of the area per lipid is far from straightforward. The area calculations involve correction terms caused by the bilayer lateral compressibility, as measured by the area compressibility modulus K_A (Needham and Evans, 1988; Rawicz et al., 2000), and shape fluctuations determined by the bending modulus K_C (Faucon et al., 1989; Méléard et al., 1997; Petrache et al., 1998b). For the benchmark lipid DPPC, these correction terms, revisited by Nagle and Tristram-Nagle (2000), increase the area at 50°C from 62.9 Å^2 to 64 Å^2, which is roughly a 1.7% increase. In the case of ^{2}H NMR data, one can introduce a correction due to ODF through a slow order parameter (Brown, 1996), as described above. We find that, with $S_{slow} = 0.7$, the calculated area decreases by only about 1.5%. In this paper, we have considered $S_{slow} = 1$, which is clearly an approximation. As a rule, the effect of ODF (and the magnitude of S_{slow}) may have an intricate behavior as a function of lipid type and temperature. We should mention that the interpretation of NMR, X-ray, and FTIR data with the help of long length scale molecular dynamics simulations, such as the one recently presented by Lindahl and Edholm (2000), could help resolve the complex issues regarding collective motions. We do not, however, expect the ODF corrections to change the results of this paper significantly. Based on ^{2}H NMR data for the homologous series of disaturated phosphatidylcholines, we have shown that, for each lipid, the thermal variation of the structural parameters is dominated by entropic effects, i.e., the acyl chains have reduced projected lengths, and occupy larger cross sectional areas as the temperature is increased. In contrast, at fixed temperature, there is a lateral condensation as the number of acyl chain segments is increased, suggesting that the additional van der Waals attraction overcomes the re-

pulsive entropic term. Concomitantly, there is a larger projected acyl length along the normal to the bilayer surface, manifesting the increased bilayer thickness as additional mass is added to the system. By altering the chain length at fixed absolute temperature, one shifts the balance of forces between the headgroup and chain interactions, and therefore alters the bilayer interfacial area.

Material properties of lipid bilayers

In this section, we further interpret the structural results from ^{2}H NMR in terms of a compact description of bilayer properties as a function of the thermodynamic variable T and the carbon number n_C (compositional variable). The material properties of the lipid bilayer can be analyzed starting from the total differential,

$$\frac{1}{V}\mathrm{d}V = \frac{1}{V}\left(\frac{\partial V}{\partial T}\right)_{\mathrm{P},n_C}\mathrm{d}T + \frac{1}{V}\left(\frac{\partial V}{\partial n_C}\right)_{\mathrm{P,T}}\mathrm{d}n_C$$

$$= \alpha\,\mathrm{d}T + \nu\,\mathrm{d}n_C\,, \tag{47}$$

which defines the isobaric volumetric expansion coefficients α and ν. The former represents the thermal expansion, whereas the latter represents the relative volume change due to additional carbons, and reduces to $\nu = 1/n_C$.

Given that $V = D_C\langle A\rangle$, we have

$$\frac{\mathrm{d}V}{V} = \frac{\mathrm{d}D_C}{D_C} + \frac{\mathrm{d}\langle A\rangle}{\langle A\rangle}, \tag{48}$$

and, in consequence, the two bulk coefficients α and ν can be each decomposed into contributions from the bilayer thickness variation (parallel component) and the lipid area variation (perpendicular component),

$$\alpha = \alpha_\parallel + \alpha_\perp\,, \tag{49}$$

and

$$\nu = \nu_\parallel + \nu_\perp\,. \tag{50}$$

Note that our definition for $\alpha_\perp$ differs by a factor of 2 from that used by Jansson et al. (1992). These coefficients, calculated from the D_C and $\langle A\rangle$ data as finite differences, are presented in Table 5 for all lipids and temperatures studied. We shall first discuss the thermal variations of the structural parameters D_C and $\langle A\rangle$ from ^{2}H NMR spectroscopy that have been presented in Fig. 8. For a given acyl chain length n_C, the hydrocarbon thickness D_C decreases, with the coefficient $\alpha_\parallel$ being on the order of -2 to $-4 \times 10^{-3}\,\mathrm{K}^{-1}$, while the interfacial area per lipid $\langle A\rangle$ increases, with the coefficient $\alpha_\perp$ between 3 and $5 \times 10^{-3}\,\mathrm{K}^{-1}$. The variation is such that there is a net volume increase on the order of $\alpha \approx 1.1\text{–}1.2 \times 10^{-3}\,\mathrm{K}^{-1}$.

The values of $\alpha_\perp$ in Table 5 compare well with the measurements of Needham and Evans (1988) on DMPC giant vesicle bilayers at similar temperatures. It is also interesting to compare $\alpha_\perp$ with the gel ($L_{\beta'}$) state values obtained by Sun et al. (1996). The comparison with the $L_{\beta'}$ state is particularly useful because the gel structure is generally better characterized in the literature. We find that the area expansivity $\alpha_\perp$ is 10 times larger in the fluid, disordered state than in the ordered gel state. For the $L_{\beta'}$ phase, Sun et al. (1996) have suggested that the reason for such a small expansion coefficient is a "competition of thermal expansion between chain packing and chain tilt." The chain lattice expansion itself is actually significant and on the order of $1.0\text{–}1.5 \times 10^{-3}\,\mathrm{K}^{-1}$, but it is counterbalanced by a decrease in the chain tilt resulting in a much smaller net change in the area per lipid (headgroup). By contrast, in the fluid state, the (static) chain tilt mechanism is absent due to higher chain disorder (and higher area per headgroup), leading to a higher $\alpha_\perp$.

We next discuss the structural results for the homologous phosphatidylcholines as a function of acyl chain length, as obtained from ^{2}H NMR spectroscopy. The relative variations of D_C and $\langle A\rangle$ with n_C are plotted in Fig. 10; the slopes of these curves are the number coefficients $\nu_\parallel$ and $\nu_\perp$ (see Table 5). The relative variations of the structural parameters

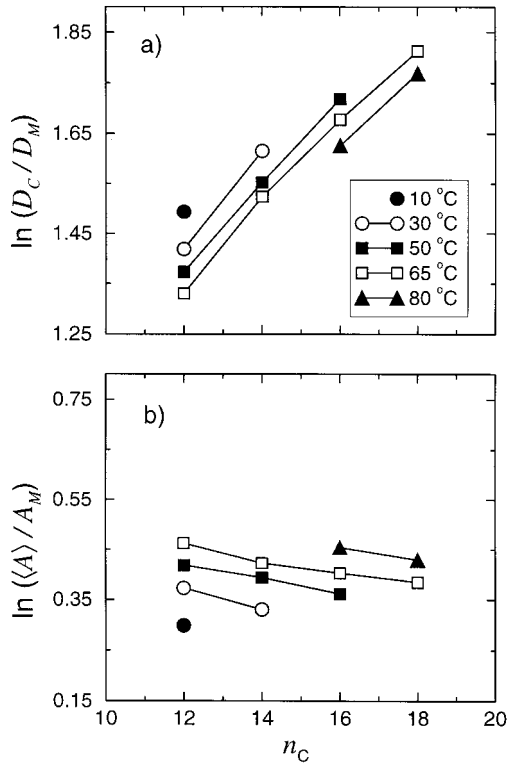

FIGURE 10 Semilogarithmic plots of relative variation of (*a*) hydrophobic thickness D_C and (*b*) area per lipid $\langle A\rangle$ as a function of acyl chain length n_C for various temperatures. D_M represents the maximum segmental projection onto the bilayer normal, and $A_M = 4V_{CH_2}/D_M$ is the corresponding minimum area. As mass is added to the hydrocarbon region, the bilayer thickness increases while the area per lipid decreases. The major influence of n_C is on the thickness rather than area.

plotted in Fig. 10, *a* and *b*, can be directly compared. It shows that the main effect of increasing the number of acyl segments is on the hydrocarbon thickness rather than on the interfacial area. The main aspect regarding the area results is that, at the same absolute temperature, the area per lipid decreases with the acyl length (i.e., $\nu_\perp$ is negative). In other words, longer chains keep the headgroups closer together, on average. The reason is that longer chains have an increased interchain van der Waals attraction that generates a reduction in the area per lipid. It is worth noting that similar behavior was found in the gel state (Sun et al., 1996), and that these observations are in agreement with the fact that longer chains have higher melting temperatures. However, as opposed to the gel state, where the lipid headgroups are in the steric interaction regime ($\langle A\rangle \approx 48$ Å^2), the lipid area in the fluid state is significantly larger due to the disordered chains (with higher chain volumes). Consequently, the headgroups are in a more elastic regime making the equilibrium area more sensitive to the temperature and acyl chain length than in the gel state (see below).

For a more detailed comparison of different chain lengths, we recall that the nonplateau order parameters for different disaturated PC lipids are practically the same at the same absolute temperature (see Fig. 3). This implies that, at fixed temperature, the segmental conformations close to the bilayer center are nearly the same for all PC lipids considered, as revealed by the Me-2-3-2 pattern in the ^{2}H NMR spectra (see above). A simple way to show this effect is to plot the relative average carbon positions $\langle z_i\rangle$ in reverse order, starting from the terminal methyl ($i = n_C$), whose position $\langle z_{n_C}\rangle$ is set to zero. The results at 65°C, calculated from the ^{2}H NMR order parameters using the first-order MT, are shown in Fig. 11 *a* and indicate that the PC lipids trace a universal curve starting at the terminal methyl and moving toward the glycerol backbone. The full extent for each lipid corresponds to L_C^* defined in Eq. 45 and given in Table 5. By contrast, the chain extension profile for DPPE, which has a different headgroup, does not fall on the same curve. Based on this observation, we conclude that the lateral packing of phospholipids is more sensitive to the headgroup methylation than to the acyl chain length. For example, the area per lipid at 65°C decreases by only 1.6% from DPPC to DSPC, but decreases by 9.8% from DPPC to DPPE. For the full chain length range studied, i.e., from DLPC to DSPC, the area decreases by 7.3%. These observations naturally lead to an interesting question: how long should the chains be for a PC lipid to approach a typical PE area? Further, what is the mechanism by which the balance of intermolecular forces shifts as a function of n_C? These are obviously central, yet difficult questions regarding our understanding of lipid assembly and microstructure. We can nevertheless attempt an heuristic description based on a phenomenological free energy form, as described in the next section.

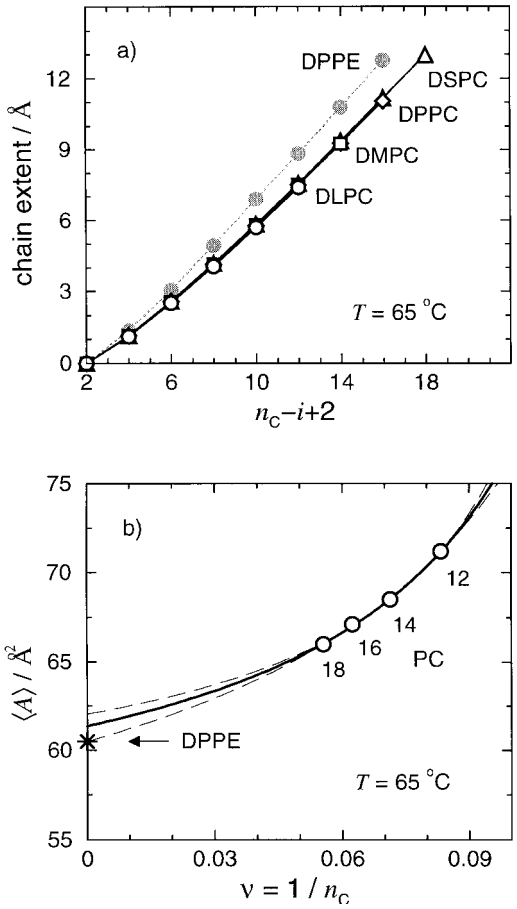

FIGURE 11 (*a*) Segmental projections onto bilayer normal starting from the terminal methyl group ($i = n_C$) and ending at the C_2 carbon ($i = 2$) at 65°C. The full extent corresponds to L_C^* from Eq. 43 and Table 5. At fixed temperature, all PC lipids follow the same curve and terminate at the corresponding chain length. Note the significantly different behavior of DPPE due to its different headgroup type. (*b*) The solid line shows a fit to $\langle A\rangle$ versus $\nu = 1/n_C$ for PC lipids (*open circles*) using Eq. 56 (*solid line*). The dashed lines show the range of uncertainty for the extrapolation at $\nu = 0$ corresponding to $A_\infty = 61.2 \pm 0.8$ Å^2. This value for A_∞ is very close to the DPPE area at 69°C (*starred symbol*), indicating that the PE headgroup allows for maximum packing of fluid acyl chains.

Balance of forces: Interfacial area of fluid bilayers

With regard to the balance of forces that dictates the equilibrium interfacial area, a free energy description in terms of material properties is most useful. For planar bilayers in general, one writes the free energy as a function of the area per lipid as (Nagle and Scott, 1978):

$$\mu(A) = \mu_0 + \left.\frac{\partial\mu}{\partial A}\right|_{A=A_0}(A - A_0) + \left.\frac{\partial^2\mu}{\partial A^2}\right|_{A=A_0}(A - A_0)^2 + \cdots$$

$$= \mu_0 + \gamma(A - A_0) + C(A - A_0)^2 + \cdots, \qquad (51)$$

where $\gamma = 0$ for a bilayer in equilibrium, and C is related to the area compressibility modulus at constant temperature,

pressure, and osmotic pressure. (The notation A_0 stands for the equilibrium area $\langle A \rangle$, and it is used for clarity in the free energy expansion.)

A simple formulation of the free energy $\mu(A)$ of a planar bilayer involves a balance of attractive and repulsive forces acting at the aqueous lipid interface (Israelachvili, 1992). The attractive components are the result of hydrophobic forces involving the hydrocarbon chains, headgroup dipolar interactions, and possibly other interactions that, in sum, give a contribution to the interfacial free energy formulated as ΓA, where Γ is a phenomenological parameter that may depend on temperature, acyl chain length, and other variables. The repulsive components are equally complex and include steric interactions, hydration forces, and entropic components due to acyl chain confinement. The effective repulsive term in the free energy is described as K/A. In terms of such a simplistic but inclusive formulation, the equilibrium area per lipid molecule $\langle A \rangle$ is dictated by the balance of opposing attractive and repulsive forces that minimizes the interfacial free energy (Israelachvili, 1992; Brown, 1994),

$$\mu(A) = \Gamma A + K/A, \tag{52}$$

leading to $\langle A \rangle = \sqrt{K/\Gamma}$.

Now from a conceptual viewpoint, one can divide the lipid bilayer into a polar headgroup region and a hydrocarbon region. It is clear that the opposing attractive and repulsive forces include contributions from both of these regions. In other words, both (phenomenological) free energy parameters Γ and K have headgroup and acyl chain components. One is therefore interested in the relative magnitude of the two contributions. For instance, it has been customarily assumed that the area per lipid is set primarily by the polar headgroup interactions, such that the chains must pack accordingly. This has indeed been shown to be the case for the lower temperature gel state of phosphatidylcholines by Sun et al. (1996), who used X-ray diffraction to accurately measure lipid packing parameters as a function of temperature and chain length (C16 to C24). It is found that, in this ordered state, the lipid headgroups are packed close to their steric limit (Tristram-Nagle et al., 1993), whereas the acyl chains are in a more elastic regime.

The equilibrium area $\langle A \rangle = \sqrt{K/\Gamma}$ can then be further interpreted in terms of individual contributions from the headgroup polar region and the hydrocarbon chains, viz. K_H, Γ_H, K_C, and Γ_C. Moreover, the hydrocarbon contribution can be considered on a per segment basis, giving $K_C = n_C k_C$ and $\Gamma_C = n_C \gamma_C$, where n_C is the number of carbon segments. Note that one can absorb the contribution of a number m of interfacial chain segments into the headgroup parameters, and redefine (offset) the pure hydrocarbon contributions as $K_C = (n_C - m)k_C$ and $\Gamma_C = (n_C - m)\gamma_C$, respectively. Using the formal head–chain partitioning of the free energy, we can write the equilibrium area as

$$\langle A \rangle = \sqrt{\frac{n_C k_C + K_H}{n_C \gamma_C + \Gamma_H}}. \tag{53}$$

Taking the logarithm and differentiating with respect to the number of carbons n_C, yields

$$\nu_\perp = \frac{1}{2}\left(\frac{k_C}{K} - \frac{\gamma_C}{\Gamma}\right), \tag{54}$$

which nicely shows how the perpendicular component of the number coefficient (given in Table 5) is related to the interaction parameters. The terms on the right-hand side each represent the fractional contributions to $\nu_\perp$ from the chains only. The first term is the fractional repulsive chain contribution, whereas the second term is the fractional attractive chain contribution. Experimentally, we find that $\nu_\perp$ is negative (on the order of -0.02), which leads to the important conclusion that

$$\frac{\gamma_C}{\Gamma} > \frac{k_C}{K}. \tag{55}$$

At given T, the fractional chain attraction is larger than the fractional chain repulsion, and the magnitude of $\nu_\perp$ indicates by how much.

Using this free energy formulation, the limiting behavior of the area per lipid is treated as follows. Starting from Eq. 53, we have

$$\langle A \rangle = \sqrt{\frac{k_C}{\gamma_C}}\sqrt{\frac{n_C + K_H/k_C}{n_C + \Gamma_H/\gamma_C}} = A_\infty \sqrt{\frac{n_C + r}{n_C + s}}$$

$$= A_\infty \sqrt{\frac{1 + r\nu}{1 + s\nu}}, \tag{56}$$

where $A_\infty = \sqrt{k_C/\gamma_C}$, $r \equiv K_H/k_C$, $s \equiv \Gamma_H/\gamma_C$, and, as before, $\nu = 1/n_C$. The advantage of using this form for the area per lipid is made clear in Fig. 11 *b*, which shows a plot of $\langle A \rangle$ versus ν at 65°C. Specifically, the extrapolation to $\nu = 0$ corresponds to the limiting area A_∞. The fit to the PC data points using the last form in Eq. 56 with three free parameters, A_∞, r, and s, is shown with the solid line. The fitted parameters are $A_\infty = 61.3 \pm 0.8$ Å^2, $r = -5.2 \pm 1.3$, and $s = -6.9 \pm 0.8$. One standard deviation in the fitted parameters is represented by the thin solid lines to show the uncertainty in the extrapolation at $\nu = 0$. The result for A_∞ is most interesting: as the acyl chain length is increased, the PC area approaches a typical PE area. How can this be explained? A parallel with the gel state behavior helps with the understanding. We recall that the PC area in the gel state is practically equal to the headgroup steric limit of about 48 Å^2, which is larger than the optimum packing for all-*trans* chains of about 40 Å^2 (Tristram-Nagle et al., 1993; Sun et al., 1996). The PE headgroup, however, allows for optimum (minimal) chain packing, as indicated by the DLPE area in

the gel state of 41 Å^2 (McIntosh and Simon, 1986). This suggests that the packing of PE lipids is dominated by chain interactions. Returning to the current fluid state data, the fit in Fig. 11 *b*, shows that the PE area represents the packing limit for fluid chains, in analogy with the gel state behavior. Thus, with regard to the equilibrium area per lipid in the fluid state, the headgroup chemical type has the greatest influence, whereas different acyl chain lengths provide for a fine tuning that generates a rich spectrum of values. This property of the lipid bilayers may modulate lipid–protein interactions and play an important role in specific biomembrane functions.

We would like to thank John F. Nagle for helpful and stimulating discussions. Thomas B. Woolf is gratefully acknowledged by H.I.P. for support and many discussions related to this work. Part of this work was conducted at the University of Würzburg, Germany, and M.F.B. is thankful to Thomas Bayerl and members of his group for generous hospitality and many valuable discussions. This work was supported by the U.S. National Institutes of Health, with additional support provided by the Röntgen-Professorship of Physics at the University of Würzburg and by the Volkswagen-Stiftung (M.F.B.).

REFERENCES

Althoff, G., N. J. Heaton, G. Gröbner, R. S. Prosser, and G. Kothe. 1996. NMR relaxation study of collective motions and viscoelastic properties in biomembranes. *Coll. Surf.* A115:31–37.

Armen, R. S., O. D. Uitto, and S. E. Feller. 1998. Phospholipid component volumes: determination and application to bilayer structure calculations. *Biophys. J.* 75:734–744.

Berger, O., O. Edholm, and F. Jähnig. 1997. Molecular dynamics simulations of a fluid bilayer of dipamitoylphosphatidylcholine at full hydration, constant pressure, and constant temperature. *Biophys. J.* 72: 2002–2013.

Bezrukov, S. M., P. R. Rand, I. Vodyanoy, and V. A. Parsegian. 1998. Lipid packing stress and polypeptide aggregation: alamethicin channel probed by proton titration of lipid charge. *Faraday Discuss.* 111: 173–183.

Bloom, M., J. H. Davis, and A. L. MacKay. 1981. Direct determination of the oriented sample NMR-spectrum from the powder spectrum for systems with local axial symmetry. *Chem. Phys. Lett.* 80:198–202.

Bloom, M., J. E. Evans, and O. G. Mouritsen. 1991. Physical properties of the fluid lipid-bilayer component of cell membranes: a perspective. *Q. Rev. Biophys.* 24:293–397.

Brown, M. F. 1982. Theory of spin-lattice relaxation in lipid bilayers and in biological membranes. ^{2}H and ^{14}N quadrupolar relaxation. *J. Chem. Phys.* 77:1576–1599.

Brown, M. F. 1994. Modulation of rhodopsin function by properties of the membrane bilayer. *Chem. Phys. Lipids.* 74:159–180.

Brown, M. F. 1996. Membrane structure and dynamics studied with NMR spectroscopy. *In* Biological Membranes, K. Merz and B. Roux, editors. Birkhäuser, Boston. 175–252.

Brown, M. F., and S. I. Chan. 1995. Bilayer membranes: deuterium & carbon-13 NMR. *In* Encyclopedia of Nuclear Magnetic Resonance. D. M. Grant and R. K. Harris, editors. Wiley, New York. 871–885.

Brown, M. F., and J. Seelig. 1977. Ion-induced changes in head group conformation of lecithin bilayers. *Nature (Lond.).* 269:721–723.

Brown, M. F., and J. Seelig. 1978. Influences of cholesterol on the polar region of phosphatidylcholine and phosphatidylethanolamine bilayers. *Biochemistry.* 17:381–384.

Chiu, S. W., M. M. Clark, E. Jakobsson, S. Subramaniam, and H. L. Scott. 1999. Application of a combined Monte Carlo and molecular dynamics method to the simulation of a dipalmitoylphosphatidylcholine lipid bilayer. *J. Comput. Chem.* 20:1153–1164.

Davies, M. A., W. Hubner, A. Blume, and R. Mendelsohn. 1992. Acyl chain conformational ordering in 1,2-dipalmitoylphosphatidylethanolamine. Integration of FT-IR and ^{2}H NMR results. *Biophys. J.* 63:1059–1062.

Davis, J. H. 1983. The description of membrane lipid conformation, order and dynamics by ^{2}H NMR. *Biophys. Biochim. Acta.* 737:117–171.

De Planque, M. R. R., D. V. Greathouse, R. E. Koeppe, H. Schäfer, D. Marsh, and J. A. Killian. 1998. Influence of lipid/peptide hydrophobic mismatch on the thickness of diacylphosphatidylcholine bilayers. A ^{2}H NMR and ESR study using designed transmembrane alpha-helical peptides and gramicidin A. *Biochemistry.* 37:9333–9345.

De Young, L. R., and K. A. Dill. 1988. Solute partitioning into lipid bilayer membranes. *Biochemistry.* 27:5281–5289.

Douliez, J.-P., A. Léonard, and E. J. Dufourc. 1995. Restatement of order parameters in biomembranes: calculation of C–C bond order parameters from C–D quadrupolar splittings. *Biophys. J.* 68:1727–1739.

Epand, R. M. 1998. Lipid polymorphism and protein–lipid interactions. *Biochim. Biophys. Acta.* 1376:353–368.

Fattal, D. R., and A. Ben-Shaul. 1995. Lipid–chain packing and lipid–protein interaction in membranes. *Physica A.* 220:192–217.

Faucon, J. F., M. D. Mitov, P. Méléard, I. Bivas, and P. Bothorel. 1989. Bending elasticity and thermal fluctuations of lipid membranes. Theoretical and experimental requirements. *J. Phys. France.* 50:2389–2414.

Feller, S. E., D. Huster, and K. Gawrisch. 1999. Interpretation of NOESY cross-relaxation rates from molecular dynamics simulations of a lipid bilayer. *J. Am. Chem. Soc.* 121:8963–8964.

Halle, B. 1991. ^{2}H NMR relaxation in phospholipid bilayers. Toward a consistent molecular interpretation. *J. Phys. Chem.* 95:6724–6733.

Huster D., K. Arnold, and K. Gawrisch. 1999. Investigation of lipid organization in biological membranes by two-dimensional nuclear overhauser enhancement spectroscopy. *J. Phys. Chem. B.* 103:243–251.

Ipsen, J. H., O. G. Mouritsen, and M. Bloom. 1990. Relationships between lipid membrane area, hydrophobic thickness, and acyl-chain orientational order. The effects of cholesterol. *Biophys. J.* 57:405–412.

Israelachvili, J. N. 1992. Intermolecular and Surface Forces. Academic Press. London.

Jansson, M., R. L. Thurmond, J. A. Barry, and M. F. Brown. 1992. Deuterium NMR study of intermolecular interactions in lamellar phases containing palmitoyllysophosphatidylcholine. *J. Phys. Chem.* 96: 9532–9544.

Koenig, W., J. A. Ferretti, and K. Gawrisch. 1999. Site-specific deuterium order parameters and membrane-bound behavior of a peptide fragment from the intracellular domain of HIV-1 gp41. *Biochemistry.* 38: 6327–6334.

Koenig, W., H. H. Strey, and K. Gawrisch. 1997. Membrane lateral compressibility determined by NMR and X-ray diffraction: effect of acyl chain polyunsaturation. *Biophys. J.* 73:1954–1966.

Lemmich, J., K. Mortensen, J. H. Ipsen, T. Hønger, R. Bauer, and O. G. Mouritsen. 1996. Small-angle neutron scattering from multilamellar lipid bilayers: theory, model, and experiment. *Phys. Rev. E.* 53: 5169–5180.

Lewis, B. A., and D. M. Engelman. 1983. Lipid bilayer thickness varies linearly with acyl chain length in fluid phosphatidylcholine vesicles. *J. Mol. Biol.* 166:211–217.

Lindahl, E., and O. Edholm. 2000. Mesoscopic undulations and thickness fluctuations in lipid bilayers from molecular dynamics simulations. *Biophys. J.* 79:426–433.

Marčelja, S. 1974. Chain ordering in liquid-crystals. II. Structure of bilayer membranes. *Biochim. Biophys. Acta.* 367:165–176.

McIntosh, T. J., and S. A. Simon. 1986. Area per molecule and distribution of water in fully hydrated dilauroylphosphatidylethanolamine bilayers. *Biochemistry.* 25:4948–4952.

Méléard, P., C. Gerbeaud, T. Pott, L. Fernandez-Puente, I. Bivas, M. D. Mitov, J. Dufourcq, and P. Bothorel. 1997. Bending elasticities of model membranes: influences of temperature and sterol content. *Biophys. J.* 72:2616–2629.

Mely, B., J. Charvolin, and P. Keller. 1975. Disorder of lipid chains as a function of their lateral packing in lyotropic liquid-crystals. *Chem. Phys. Lipids.* 15:161–173.

Mendelsohn, R., M. A. Davies, J. W. Brauner, H. F. Schuster, and R. A. Dluhy. 1989. Quantitative determination of conformational disorder in the acyl chains of phospholipid bilayers by infrared spectroscopy. *Biochemistry.* 28:8934–8939.

Meraldi, J.-P., and J. Schlitter. 1981. A statistical mechanical treatment of fatty acyl chain order in phospholipid bilayers and correlation with experimental data. *Biochim. Biophys. Acta.* 645:183–192.

Morrow, M. R., J. P. Whitehead, and D. Lu. 1992. Chain-length dependence of lipid bilayer properties near the liquid crystal to gel phase transition. *Biophys. J.* 63:18–27.

Nagle, J. F. 1980. Theory of the main lipid bilayer phase transition. *Ann. Rev. Phys. Chem.* 31:157–195.

Nagle, J. F. 1993. Area/lipid of bilayers from NMR. *Biophys. J.* 64: 1476–1481.

Nagle, J. F., and H. L. Scott. 1978. Lateral compressibility of lipid mono- and bilayers. Theory of membrane permeability. *Biochim. Biophys. Acta.* 513:236–243.

Nagle, J. F., and S. Tristram-Nagle. 2000. Structure of lipid bilayers. *Biochim. Biophys. Acta.* In press.

Nagle, J. F., and M. C. Wiener. 1988. Structure of fully hydrated bilayer dispersions. *Biochim. Biophys. Acta.* 942:1–10.

Nagle, J. F., and D. A. Wilkinson. 1978. Lecithin bilayers: density measurements and molecular interactions. *Biophys. J.* 23:159–175.

Nagle, J. F., R. Zhang, S. Tristram-Nagle, W.-J. Sun, H. I. Petrache, and R. M. Suter. 1996. X-ray structure determination of fully hydrated L_α phase dipalmitoylphosphatidylcholine bilayers. *Biophys. J.* 70: 1419–1431.

Needham, D., and E. Evans. 1988. Structure and mechanical properties of giant lipid (DMPC) vesicle bilayers from 20°C below to 10°C above the liquid crystal-crystalline phase transition at 24°C. *Biochemistry.* 27: 8261–8269.

Nevzorov, A. A., T. P. Trouard, and M. F. Brown. 1998. Lipid bilayer dynamics from simultaneous analysis of orientation and frequency dependence of deuterium spin-lattice and quadrupolar order relaxation. *Phys. Rev. E.* 58:2259–2281.

Oldfield, E., M. Meadows, D. Rice, and R. Jacobs. 1978. Spectroscopic studies of specifically deuterium labeled membrane systems. Nuclear magnetic resonance investigation of effects of cholesterol in model systems. *Biochemistry.* 17:2727–2740.

Pastor, R. W., and S. E. Feller. 1996. Time scales of lipid dynamics and molecular dynamics. *In* Biological Membranes. K. Merz and B. Roux, editors. Birkhäuser, Boston. 3–29.

Pastor, R. W., R. M. Venable, and M. Karplus. 1988. Brownian dynamics simulation of a lipid chain in a membrane bilayer. *J. Chem. Phys.* 89:1112–1127.

Pastor, R. W., R. M. Venable, and M. Karplus. 1990. Model for the structure of the lipid bilayer. *Proc. Natl. Acad. Sci. USA.* 88:892–896.

Petrache, H. I., S. E. Feller, and J. F. Nagle. 1997. Determination of component volumes from simulations. *Biophys. J.* 72:2237–2242.

Petrache, H. I., S. Tristram-Nagle, and J. F. Nagle. 1998a. Fluid phase structure of EPC and DMPC bilayers. *Chem. Phys. Lipids.* 95:83–94.

Petrache, H. I., N. Gouliaev, S. Tristram-Nagle, R. Zhang, R. M. Suter, and J. F. Nagle. 1998b. Interbilayer interactions from high resolution X-ray scattering. *Phys. Rev. E.* 57:7014–7024.

Petrache, H. I., K. Tu, and J. F. Nagle. 1999. Analysis of simulated NMR order parameters for lipid bilayer structure determination. *Biophys. J.* 76:2479–2487.

Rand, R. P., and V. A. Parsegian. 1989. Hydration forces between phospholipid bilayers. *Biochim. Biophys. Acta.* 988:351–376.

Rawicz, W., K. C. Olbrich, T. McIntosh, D. Needham, and E. Evans. 2000. Effect of chain length and unsaturation on elasticity of lipid bilayers. *Biophys. J.* 79:328–339.

Salmon, A., S. W. Dodd, G. D. Williams, J. M. Beach, and M. F. Brown. 1987. Configurational statistics of acyl chains in polyunsaturated lipid bilayers from ^{2}H NMR. *J. Am. Chem. Soc.* 109:2600–2609.

Schindler, H., and J. Seelig. 1975. Deuterium order parameters in relation to thermodynamic properties of a phospholipid bilayer. *Biochemistry.* 14:2283–2287.

Scott, H. L. 1986. Monte Carlo calculations of order parameter profiles in models of lipid–protein interactions in bilayers. *Biochemistry.* 25: 6122–6126.

Seelig, J. 1977. Deuterium magnetic resonance: theory and application to lipid membranes. *Q. Rev. Biophys.* 10:353–418.

Seelig, A., and J. Seelig. 1974. The dynamic structure of fatty acyl chains in a phosphatidylcholine bilayer measured by deuterium magnetic resonance. *Biochemistry.* 13:4839–4845.

Smondyrev, A. M., and M. L. Berkowitz. 1999. Molecular dynamics study of Sn-1 and Sn-2 chain conformations in DPPC membranes. *J. Chem. Phys.* 110:3981–3985.

Sun, W.-J., R. M. Suter, M. A. Knewtson, C. R. Worthington, S. Tristram-Nagle, R. Zhang, and J. F. Nagle. 1994. Order and disorder in fully hydrated unoriented bilayers of gel phase DPPC. *Phys. Rev. E.* 49: 4665–4676.

Sun, W.-J., S. Tristram-Nagle, R. M. Suter, and J. F. Nagle. 1996. Structure of gel phase saturated lecithin bilayers: temperature and chain length dependence. *Biophys. J.* 71:885–891.

Tardieu, A., V. Luzzati, and F. C. Reman. 1973. Structure and polymorphism of the hydrocarbon chains of lipids: a study of lecithin-water phases. *J. Mol. Biol.* 75:711–733.

Thurmond, R. L., S. W. Dodd, and M. F. Brown. 1991. Molecular areas of phospholipids as determined by ^{2}H NMR spectroscopy. Comparison of phosphatidylethanolamines and phosphatidylcholines. *Biophys. J.* 59: 108–113.

Tristram-Nagle, S., H. I. Petrache, and J. F. Nagle. 1998. Structure and interactions of fully hydrated dioleoylphosphatidylcholine bilayers. *Biophys. J.* 75:917–925.

Tristram-Nagle, S., R. Zhang, R. M. Suter, C. R. Worthington, W.-J. Sun, and J. F. Nagle. 1993. Measurement of chain tilt angle in fully hydrated bilayers of gel phase lecithins. *Biophys. J.* 64:1097–1109.

Trouard, T. P., T. M. Alam, and M. F. Brown. 1994. Angular dependence of deuterium spin-lattice relaxation rates of macroscopically oriented dilauroylphosphatidylcholine in the liquid-crystalline state. *J. Chem. Phys.* 101:5229–5261.

Trouard, T. P., T. M. Alam, J. Zajicek, and M. F. Brown. 1992. Angular anisotropy of ^{2}H NMR spectral densities in phospholipid bilayers containing cholesterol. *Chem. Phys. Lett.* 189:67–75.

Trouard, T. P., A. A. Nevzorov, T. M. Alam, C. Job, J. Zajicek, and M. F. Brown. 1999. Influence of cholesterol on dynamics of dimyristoylphosphatidylcholine bilayers as studied by deuterium NMR relaxation. *J. Chem. Phys.* 110:8802–8818.

Tuchtenhagen, J., W. Ziegler, and A. Blume. 1994. Acyl chain conformational ordering in liquid-crystalline bilayers: comparative FT-IR and ^{2}H-NMR studies of phospholipids differing in headgroup structure and chain length. *Eur. Biophys. J.* 23:323–335.

White, S. H., and W. C. Wimley. 1999. Membrane protein folding and stability: physical principles. *Annu. Rev. Biophys. Biomol. Struct.* 28: 319–365.

Wiener, M. C., and S. H. White. 1992. Structure of fluid DOPC determined by joint refinement of X-ray and neutron diffraction data. III. Complete structure. *Biophys. J.* 61:434–447.

Williams, G. D., J. M. Beach, S. W. Dodd, and M. F. Brown. 1985. Dependence of deuterium spin-lattice relaxation rates of multilamellar phospholipid dispersions on orientational order. *J. Am. Chem. Soc.* 24:6868–6873.

Worthington, C. R., G. I. King, and T. J. McIntosh. 1973. Direct structure determination of multilayered membrane-type systems which contain fluid layers. *Biophys. J.* 13:480–494.

Xu, Z.-C., and D. S. Cafiso. 1986. Phospholipid packing and conformation in small vesicles revealed by two-dimensional ^{1}H nuclear magnetic resonance cross-relaxation spectroscopy. *Biophys. J.* 49:779–783.

Zaccai, G., G. Büldt, A. Seelig, and J. Seelig. 1979. Neutron diffraction studies on phosphatidylcholine model membranes. II. Chain conformation and segmental disorder. *J. Mol. Biol.* 134:693–706.